Oxygen is a critical regulator of cellular metabolism and function in cell culture

Joycelyn Tan[1,15], Sam Virtue[1,15,*], Dougall M. Norris[1,15], Olivia J. Conway[1], Ming Yang[2,3], Christopher Gribben[4], Fatima Lugtu[4], James R. Krycer[5,6], Richard J. Mills[5,6], Ioannis Kamzolas[1,7], Conceição Pereira[8], Martin Dale[1], Amber S. Shun-Shion[1], Harry J. M. Baird[1], James A. Horscroft[9], Alice P. Sowton[9], Marcella Ma[1], Stefania Carobbio[1,10], Evangelia Petsalaki[7], Andrew J. Murray[9], David C. Gershlick[8], James E. Hudson[5,6,11], Ludovic Vallier[4], Kelsey H. Fisher-Wellman[12,13,14], Christian Frezza[2,3], Antonio Vidal-Puig[1,10,*], Daniel J. Fazakerley[1,16,*]

[1]Metabolic Research Laboratories, Wellcome-Medical Research Council Institute of Metabolic Science, University of Cambridge, Cambridge CB2 0QQ, UK.
[2]MRC Cancer Unit, University of Cambridge, Cambridge Biomedical Campus, Cambridge CB2 0XZ, UK.
[3]CECAD Research Center, Faculty of Medicine, University Hospital Cologne, Cologne 50931, Germany.
[4]Wellcome-MRC Cambridge Stem Cell Institute, University of Cambridge, Cambridge CB2 0AW, UK.
[5]QIMR Berghofer Medical Research Institute, Brisbane, Queensland 4006, Australia.
[6]Faculty of Health, School of Biomedical Sciences, Queensland University of Technology, Brisbane, Queensland 4000, Australia.
[7]European Molecular Biology Laboratory, European Bioinformatics Institute, Wellcome Genome Campus, Hinxton CB10 1SD, UK.
[8]Cambridge Institute for Medical Research, University of Cambridge, Cambridge CB2 0XY, UK.
[9]Department of Physiology, Development and Neuroscience, University of Cambridge, Cambridge CB2 3EL, UK.
[10]Centro de Investigacion Principe Felipe, Valencia 46012, Spain.
[11]Faculty of Medicine, School of Biomedical Sciences, The University of Queensland, Brisbane, Queensland 4072, Australia.
[12]Department of Physiology, Brody School of Medicine, East Carolina University, Greenville, North Carolina 27834, USA.
[13]East Carolina Diabetes and Obesity Institute, East Carolina University, Greenville, North Carolina 27834, USA.
[14]UNC Lineberger Comprehensive Cancer Center, University of North Carolina at Chapel Hill School of Medicine, Chapel Hill, North Carolina 27599, USA.
[15]These authors contributed equally
[16]Lead Contact
*Correspondence: djf72@medschl.cam.ac.uk (Daniel Fazakerley); ajv22@medschl.cam.ac.uk (Antonio Vidal-Puig); sv234@medschl.cam.ac.uk (Sam Virtue)

SUMMARY

Cell culture, the workhorse of biomedical research, is generally considered to be hyperoxic. However, oxygen consumption by cells is underappreciated. High cellular respiration rates can rapidly deplete oxygen, resulting in local hypoxia. Increasing pericellular oxygen levels rewired the metabolism of multiple post-mitotic cell-lines, both in monolayer and organoid culture. Under standard conditions, cultured adipocytes are hypoxic and highly glycolytic. Increased oxygen availability diverted glucose flux toward mitochondria and increased lipogenesis from glucose-derived carbon. These metabolic changes were coupled to thousands of gene expression changes, and rendered adipocytes more sensitive to insulin and lipolytic stimuli. Importantly, pathway analyses revealed increasing oxygen tension made *in vitro* adipocytes more similar to *in vivo* adipose tissue. hPSC-derived hepatocytes and cardiac organoids were also functionally enhanced by increased oxygen. Our findings suggest that oxygen is limiting in many standard cell culture systems, and highlight how controlling oxygen availability can improve translatability of cell models.

Keywords: Cell culture, oxygen tension, oxygen diffusion, hypoxia, HIF, glucose metabolism, *de novo* lipogenesis, adipocytes, hPSC

INTRODUCTION

Cell culture is often described as a state of artificially high oxygen tension[1]. This assumption is based on the fact that cell culture incubators are usually between 90 and 95% air (the rest being CO_2 and water vapour), meaning that the oxygen tension at the culture medium surface is approximately 140 mmHg at sea level (18.5% O_2). Therefore, the maximum O_2 saturation in cell culture medium is 181 µM (at 37ºC, 5% CO_2), substantially higher than the oxygen tension human tissues are exposed to, which ranges between 6.5-130 µM. However, the "assumption of hyperoxia" ignores oxygen consumption by cells[2]. Depending on the cell type, oxygen consumption rates can vary by up to 60-fold[2]. As a result, there is a decreasing oxygen gradient between the media surface and cell monolayer[3,4]. The steepness of this gradient is highly cell-type specific, and results in hypoxia in some cell lines[5-7]. Despite these reports, pericellular oxygen tension remains a neglected consideration during cell culture, with most researchers likely unaware of whether their cells cultured under standard conditions are hyperoxic, normoxic, or hypoxic. This is likely a result of the almost complete lack of data on the impact of low pericellular oxygen tension under "standard culture conditions" on cellular phenotypes and the translatability of culture models.

Hypoxic and anoxic states promote anaerobic glycolytic metabolism both *in vivo* and *in vitro*. Consistent with the idea that cell culture could be hypoxic, many cultured cells are reported to be highly glycolytic, generating lactate from glucose[8-11]. However, perhaps due to the fact most cell lines are highly proliferative, this glycolytic metabolism is often attributed to an intrinsic metabolic rewiring of cultured cells, similar to the aerobic glycolysis observed in cancer cells due to the Warburg effect. A second suggestion for the high rates of glycolysis is that it occurs as a result of the use of unphysiological media[12-17]. As such, the relevance of results obtained from cell culture to *in vivo* metabolism is often debated, with the metabolism of cells in culture being analogous to tumour metabolism, even in the presence of supposedly artificially high oxygen tension[18]. However, an arguably simpler explanation for the high glycolytic rates of many cultured cells is that oxygen is limiting; with cells responding physiologically to a hypoxic environment.

Here we provide experimental evidence that multiple metabolic cell lines are hypoxic under standard culture conditions, and explore the consequences of limited oxygen availability on cellular metabolism and phenotypes. We show that the high glycolytic activity of many cultured cell lines is a physiological response to hypoxia, resulting from limitations in oxygen diffusion from the air through the medium column to the base of the cell culture plate. We demonstrate

that increasing oxygen availability reprogrammed cells away from glycolytic and toward oxidative metabolism, increased pyruvate dehydrogenase (PDH) flux, tricarboxylic acid (TCA) cycle activity and oxygen consumption, promoted lipid anabolism, destabilising hypoxia-inducible factor (HIF) 1α protein and inducing over 3000 transcriptional changes within 16 h. Notably, these changes occurred in multiple cell lines and resulted in phenotypic changes that rendered cells more similar to *in vivo* tissues. Our findings highlight the importance of understanding and controlling oxygen availability in cell culture models to better model *in vivo* tissues.

RESULTS AND DISCUSSION

Increasing pericellular oxygen tension decreases lactate production and increases *de novo* lipogenesis in 3T3-L1 adipocytes

To study the effects of oxygen tension in cell culture we selected the 3T3-L1 adipocyte cell line as our primary model. 3T3-L1 adipocytes are generated from a fibroblast precursor cell line[19] and are commonly used to study adipocyte differentiation[20-22] lipid metabolism[23] and hormonal responses[24]. Under standard culture conditions (e.g., 1 mL DMEM/10% FCS per well in 12-well plates) (Figure S1A) 3T3-L1 adipocytes grow as a monolayer and produce high levels of lactate[8] (Figure 1A). Given the high oxygen consumption rate (OCR) (200 fmol/mm^2/s) of 3T3-L1 adipocytes (Figures 1B and 1C), we hypothesised that their glycolytic phenotype may not be innate, but a consequence of limited oxygen availability. Fick's first law of gas diffusion (Figure 1D) states that oxygen diffusion rates are proportionate to medium depth. To support an OCR of 200 fmol/mm^2/s we calculated that medium depth could not exceed 2.43 mm (e.g., a 5 mm medium depth would limit OCR to just 100 fmol/mm^2/s). Medium height is not constant in cell culture wells due to the meniscus. The minimum depth of medium in a 12-well plate containing 1 mL of medium was measured at ~2.4 mm (see Figures 1D and S1A). Based on the OCR of 3T3-L1s, Fick's law predicts that oxygen concentrations at the cell monolayer would be virtually 0[25]. Indeed, under standard culture conditions (100 µL per well in a 96-well plate), the oxygen concentration measured 0.55 mm above the cell monolayer (the minimum measurable depth by the Resipher system) was ~15 µM (1.5% O$_2$) (Figures 1E and S1A), well below atmospheric oxygen (181 µM; 18.5% O$_2$). To increase oxygen tension at the cell monolayer, we lowered medium volumes, reducing the distance from the air-media interface to the cell monolayer (Figure 1D). As expected, lowering medium volumes increased O$_2$ at the cell monolayer (Figure S1B), with oxygen concentrations 0.55 mm above the cell monolayer reaching between 38 µM and 73 µM for cells cultured in 50 µL or 33 µL medium in a 96-well plate, respectively (Figure 1E). Therefore, lowering medium volumes provided a simple experimental system to assess the impact of oxygen tension on 3T3-L1 adipocyte metabolism[26].

Under low oxygen tension, glycolysis switches from being primarily aerobic, with CO$_2$ as the end point, to becoming increasingly anaerobic, with lactate as the end point. We initially measured glucose consumption and lactate production. Switching cells cultured in 12-well plates from 1 mL (high) to 0.67 mL (mid) or 0.33 mL (low) medium lowered glucose uptake and caused an even more drastic reduction in lactate production (Figure 1A). This was not driven by depletion of glucose, which remained > 12 mM under all medium volumes after 16 h (Figure S1C). Instead, our results indicated a large reduction in anaerobic glycolysis under conditions of greater oxygen availability (Figure 1A). Critically, despite a 50% reduction in glucose uptake, cells cultured in lower medium volumes (0.33 mL *versus* 1 mL) increased *de novo* lipogenesis (DNL) (Figure 1F), indicating the cells were substantially more metabolically efficient; able to produce sufficient ATP and obtain enough carbon to support DNL from less glucose. Indeed, that the cells were doing more with less can be rationalised by glucose metabolism to lactate generating 2 molecules of ATP, whereas the complete oxidation of glucose in mitochondria generates up to 36[27]. To confirm that these metabolic responses to low medium conditions were due to a primary change in oxygen availability, we cultured cells in gas-permeable cell culture plates (Lumox) that allow oxygen diffusion from the bottom of

the well. Similar to the low medium conditions, gas-permeable plates lowered glucose use and lactate production (Figure 1G) and increased DNL (Figure 1H). Overall, these results demonstrated that the glycolytic metabolism of 3T3-L1 cells was not innate, but a response to limited oxygen supply. We next sought to determine how important the impact of increasing oxygen tension was to the metabolism and phenotypes of cells in culture.

Lowering medium volumes increases mitochondrial glucose oxidation
We next directly measured OCR under different medium volumes. Switching cells from standard (100 µL per well in 96-well plates) to low (33 µL) medium conditions rapidly (within 3-4 h) doubled the oxygen consumption rate from 200 to 400 fmol/mm^2/s (Figure 2A), showing that standard culture volumes were indeed limiting for 3T3-L1 adipocyte oxygen consumption. This was independent of changes in mitochondrial content as measured by western blotting (Figure S2A) or oxygen consumption in permeabilised cells (Figure S2B). Under standard culture conditions, medium oxygen concentration was ~15 µM 0.55 mm above the cells (Figure 1E). However, in a closed system, 3T3-L1 adipocytes respired maximally down to ~4 µM (<0.3% O$_2$) oxygen (Figure 2B). Together, these data suggest a near total use of available oxygen (to less than 4 µM) at the cell monolayer. Overall, we demonstrate that, under standard culture conditions, 3T3-L1 adipocytes consume all oxygen that diffuses to the monolayer, become hypoxic, and perform anaerobic glycolysis to maximise ATP production.

Multiple adaptations to hypoxia are known, including increased glucose uptake for anaerobic glycolysis[28], inhibition of PDH flux to limit aerobic TCA cycle activity[29], and activation of the HIF system[30,31]. Firstly, we determined changes in glucose transport and expression of glucose transporters. We did not see any changes in the protein levels of the insulin-regulated glucose transporter GLUT4. In contrast, the hypoxia-inducible glucose transporter GLUT1 was strongly suppressed by low medium, as was non-GLUT4 dependent glucose uptake (Figures 2C and S2C). Second, PDH phosphorylation was decreased following the switch to low medium volumes (Figure 2D), consistent with decreased negative regulation of PDH by pyruvate dehydrogenase kinases (PDKs) and therefore increased PDH activity[29,32]. Indeed, direct measurement of PDH flux using mass isotopomer distribution analysis (MIDA) of palmitate[33] revealed a ~40% increase in glucose entry to the TCA cycle via PDH when cells were cultured in lower medium volumes (Figure 2E). Consistent with greater PDH activity and glucose entry into the TCA cycle, U^{13}C-glucose tracing (Figure 2F) revealed that transitioning cells to low medium (0.33 mL in 12-well plates) for either 4 h (Figure S2E) or 16 h (Figure 2G) increased ^{13}C-labelling of all TCA cycle intermediates (Table S1). Additionally, enrichment of m+3 isotopologues for fumarate and malate suggested increased pyruvate carboxylase activity, which allows for TCA anaplerosis by replenishing oxaloacetate. In total, the abundance of 45 metabolites was changed by culturing cells in low medium for 16 h, indicating comprehensive metabolic rewiring of cells beyond just the TCA cycle (Figure S2G). Of note, α-ketoglutarate (α-KG) was the most upregulated TCA metabolite under low medium conditions (Figure S2F), with all the additional α-KG containing glucose-derived carbon (Figure 2H). These results demonstrate that increasing oxygen tension can rewire multiple branches of cell metabolism in addition to increased glucose oxidation via the TCA cycle.

Lowering medium volumes induces a widespread transcriptional response and improves adipocyte function
Changes in α-KG abundance, which governs the activity of α-KG-dependent dioxygenase prolyl hydroxylases[34-36], alongside changes in cellular oxygen tension, and lower GLUT1 protein levels[37] are all indicative of reduced HIF1α stability and decreased transcriptional activity. We first determined if transitioning cells from high to low medium altered HIF1α stabilisation. HIF1α abundance was drastically decreased when cells were switched to low medium for 16 h (Figure 3A). Accordingly, expression of HIF1α target genes (*Slc16a3, Pgk1, Pdk1, Car9, Pkm2, Slc2a1*) was also reduced under low medium conditions (Figure 3B) and in cells cultured in gas-permeable culture plates (Lumox) (Figure S3A). To fully characterise the transcriptional responses to low medium we performed RNAseq analyses. This revealed

extensive and widespread changes in gene expression in cells cultured in low medium, with over 3000 differentially expressed genes. Multiple HIF1α targets were expressed at greater levels in high medium (Figure 3C; Table S2). VIPER transcription factor prediction software predicted 125 transcription factors to either be inhibited or activated (Table S3) by changing medium volume, including HIF1α (NES 8.8, FDR P-value=1.6 10^{-16}). Finally, FGSEA identified 63 altered KEGG pathways (Table S4). Notably, mitochondrial function, TCA cycle activity, and lipogenesis, were all predicted to be increased by low medium (Table S4), consistent with our biochemical analyses (Figures 1 and 2).

The extensive changes in gene expression suggested that increased oxygen availability to cells may have broader implications than altered glucose metabolism. Therefore, we next tested cellular phenotypes relevant to adipocyte biology including adipokine secretion, insulin responsiveness, and lipolysis. We cultured adipocytes in high or low medium for 48 h, during which their metabolic switch to glucose oxidation in low medium was maintained (Figure S3B). At this time point, low medium increased both leptin and adiponectin secretion (Figures 3D and 3E), consistent with gene expression data for *Lepn* and *AdipoQ* (Table S2). Additionally, low medium markedly increased insulin-stimulated GLUT4 translocation at both physiological and supraphysiological insulin concentrations (Figure 3F). Similarly, while total 2-deoxyglucose (2-DG) uptake in the presence of insulin was similar in cells cultured in low or high medium volumes, the treatment of cells with the GLUT4-inhibitor indinavir demonstrated that 2-DG uptake was more GLUT4-dependent in low medium (Figure S2D), despite no changes in total GLUT4 protein (Figure 2C).

While adipokine secretion and insulin-stimulated glucose uptake are important functions of mature adipocytes, the primary role of adipose tissue is the storage and mobilisation of fat. Extended culture in low medium increased the sensitivity of 3T3-L1 adipocytes to the lipolysis-stimulating β3-adrenergic receptor agonist CL316,243 more than 15-fold (EC_{50} 0.21 nM *versus* 3.43 nM) (Figure 3G). Despite higher lipolytic sensitivity, insulin was equally effective at suppressing lipolysis in response to CL316,243 (Figure 3H). Overall, these phenotypic measures suggested that increased oxygen tension improved endocrine, glucose and lipid metabolic functions in 3T3-L1 adipocytes. The powerful effects of adjusting oxygen tension highlight the need for researchers to control and report on factors that impact oxygen tension (e.g., media volumes, cell densities, respiration rate) to ensure reproducibility.

Given the improvement in adipocyte function in response to greater oxygen tension, we next compared our *in vitro* findings to *in vivo* adipose tissue. We compared the transcriptional profile of 3T3-L1 adipocytes in low *versus* high medium culture conditions to subcutaneous white adipose tissue (scWAT) from mice exposed to either normoxia (21% O_2) or hypoxia (10% O_2, 4 weeks) (Figure S3C, Tables S5 and S6). Both individual gene and pathway analyses revealed a high degree of overlap in gene expression responses of cells cultured in high medium and hypoxic adipose tissue. Specifically, of the 2239 differentially expressed genes in hypoxic mice scWAT, 703 were also changed in the 3T3-L1 adipocytes cultured in high medium (Figure S3D), with a 77% concordance in the direction of change (Fig S3E). Additionally, out of 312 KEGG pathways tested, 63 were significantly altered in 3T3-L1 adipocytes and 61 in scWAT, of which 34 were significant in both (Chi^2 for overlap p=6*10E^{-11}) (Table S4 and S6). Remarkably, 32 of the 34 common pathways were concordantly regulated (Figure 3I, Table S4 and S6). Overall, our data suggested that "standard" culture conditions mimic hypoxic adipose tissue and that increasing oxygen tension better modelled normoxic adipose tissue.

Lowering medium volumes reduces lactate production and improves functional outcomes in other cell types and organoids

Finally, we extended our analysis to other cell types/tissues. First, we assessed lactate secretion in other post-mitotic cell lines cultured under high or low medium volume conditions. pBAT cells (murine brown adipocytes) and L6 myotubes (rat) responded to lower medium

volumes by significantly reducing lactate secretion (Figure 4A). Next, we extended our studies to assess the functional effects of increasing oxygen tension in human pluripotent stem cells (hPSC)-derived hepatocytes and cardiac organoids. Induced pluripotent stem cells (iPSC)-derived hepatocytes lowered lactate secretion when cultured in low medium (Figure 4B) and lowered HIF1α target gene expression (Fig S4A). Transition to low medium altered mRNA levels of hepatocyte differentiation markers by increasing the mature hepatocyte markers *ALB* (albumin) and, *SERPINA1*, and decreasing the lineage specification marker *HNF4α*[38,39] (Figure 4C). On a protein level, we observed increased CYP3A4 activity and hepatocyte albumin content (Figures 4D and 4E). The powerful reduction in HIF1α target gene expression (Figure S4A) indicated that lowering medium volumes may help in the differentiation of functional hepatocytes from iPSCs[40,41]. hPSC-derived cardiac organoid cultures also secreted less lactate when cultured in lower medium volumes (Figures 4F and S4B). Organoids in low medium exhibited greater contractile force (Figure 4G), without changes in contractile rate, or activation and relaxation times. (Figures S4C–E). Our data suggest that manipulating oxygen tension, at least in terminally differentiated cells that model major metabolic organs, impacts the metabolism and phenotype of multiple different cell types. It is notable that air−liquid interface (ALI) culture models have been adopted for many stem-cell and organoid lines, including the respiratory tract[42], brain[43], tumour immune microenvironment[44], and gastrointestinal tissues[45]. Our results regarding the impact of media depth offer a compelling explanation for the efficacy of these air-liquid interface systems and ultimately provide a rationale to allow further improvements to hPSC-based models.

This study highlights that cell culture is not a state of artificially high oxygen tension. Instead, it is a state of variable oxygen tension. Manipulating oxygen levels has dramatic effects on many aspects of cellular metabolism and function, with important implications for the translatability of both cell and tissue culture models to *in vivo* settings.

ACKNOWLEDGMENTS

AUTHOR CONTRIBUTIONS

Conceptualisation (S.V., D.M.N., and D.J.F.), methodology (J.T., S.V., D.M.N., A.S.S., and D.J.F.), formal analysis (J.T., S.V., M.Y., and I.K.), investigation (J.T., S.V., D.M.N., O.J.C., M.Y., C.G., F.L., J.R.K., I.K., C.P., M.D., H.J.M.B., J.A.H., A.P.S., E.N., M.M., S.C., E.P., A.J.M., D.C.G., J.E.H., L.V., K.H.F-W., and D.J.F.), writing of manuscript (J.T., S.V., and D.J.F.,

with inputs from all authors), visualisation (J.T., S.V., M.Y., K.H.F-W., and J.E.H.), supervision (S.V., E.P., A.J.M., D.C.G., J.E.H., L.V., C.F., A.V-P., and D.J.F.), project administration (J.T., S.V., and D.J.F.).

DECLARATION OF INTERESTS

The authors declare that they have no competing interests.

RIGHTS RETENTION STATEMENT

This work was funded by a UKRI grant (MR/S007091/1). For the purpose of open access, the author has applied a Creative Commons Attribution (CC BY) licence to any Author Accepted Manuscript version arising.
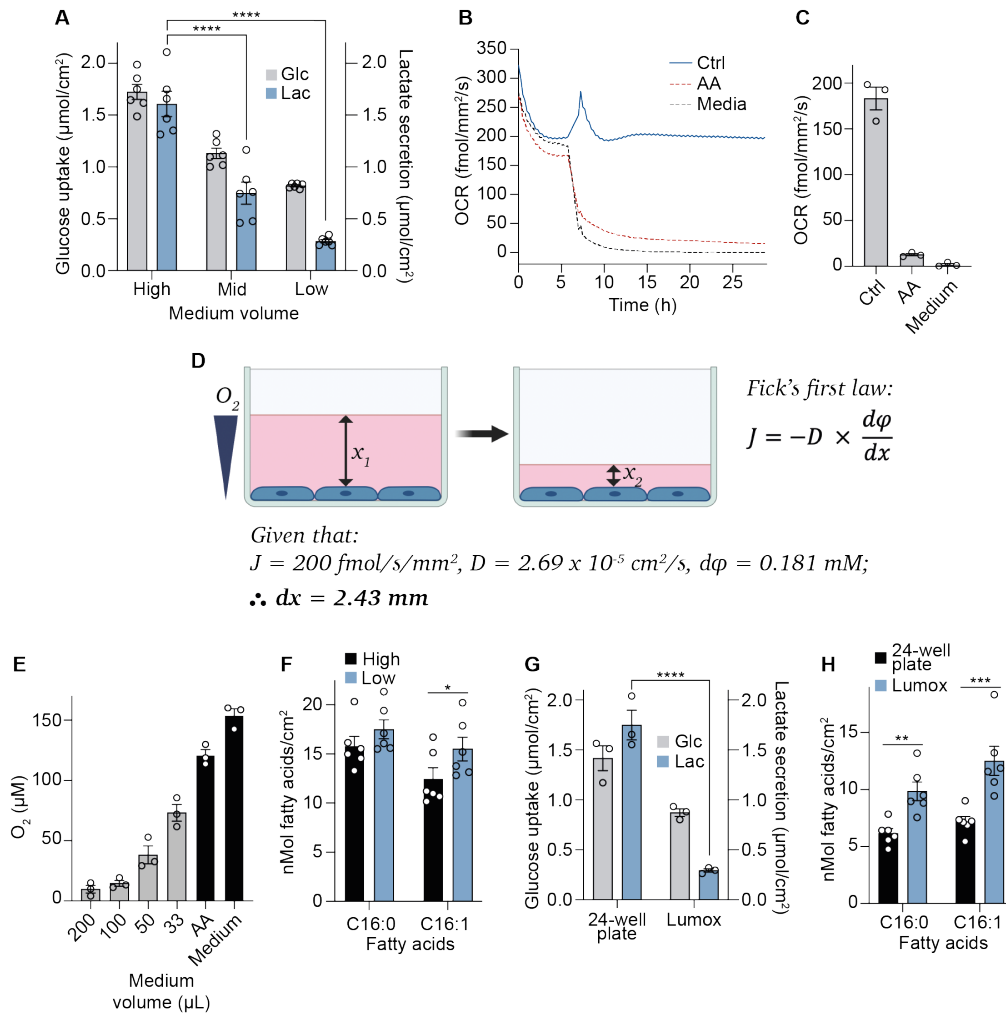
Figure 1. Increasing pericellular oxygen tension decreases lactate production and increases *de novo* lipogenesis in 3T3-L1 adipocytes

(A) Extracellular medium glucose and lactate measurements 16 h after medium volume change. High = 1 mL, Mid = 0.67 mL, Low = 0.33 mL from hereafter unless stated otherwise. (n = 6 biological replicates).

(B) 3T3-L1 adipocyte oxygen consumption rate (OCR) under control (100 µL), mitochondrial complex III inhibitor antimycin A (AA) treatment, or cell-free/medium only conditions. Baseline OCR was measured for 6 h before starting AA treatment and removing cells from medium-only wells (representative of n = 3 biological replicates).

(C) OCR measurements taken after 20 h from (B) (n = 3 biological replicates).

(D) Schematic representation of experimental setup and Fick's first law of diffusion, which states that the rate of diffusion (*J*) is proportional to the concentration gradient (φ) and is inversely proportional to the diffusion length (*x*), where *D* is the diffusion coefficient.

(E) Pericellular oxygen concentration at different medium volumes (n = 3 biological replicates).

(F) *De novo* lipogenesis (DNL) of palmitate (C16:0) and palmitoleate (C16:1) during 16 h of culture in high or low medium volumes (n = 6 biological replicates)

(G) Extracellular medium glucose and lactate measurements in 24-well or Lumox plates after 16 h (n = 3 biological replicates).

(H) DNL of palmitate and palmitoleate after 16 h in 24-well or gas-permeable Lumox plates (n = 6 biological replicates)

Data are represented as mean ± SEM. *$p < 0.05$, **$p < 0.01$, ***$p < 0.001$, ****$p < 0.0001$ by two-way ANOVA with Šidák correction for multiple comparisons (A, E, F, G, and H).

See also Figure S1.
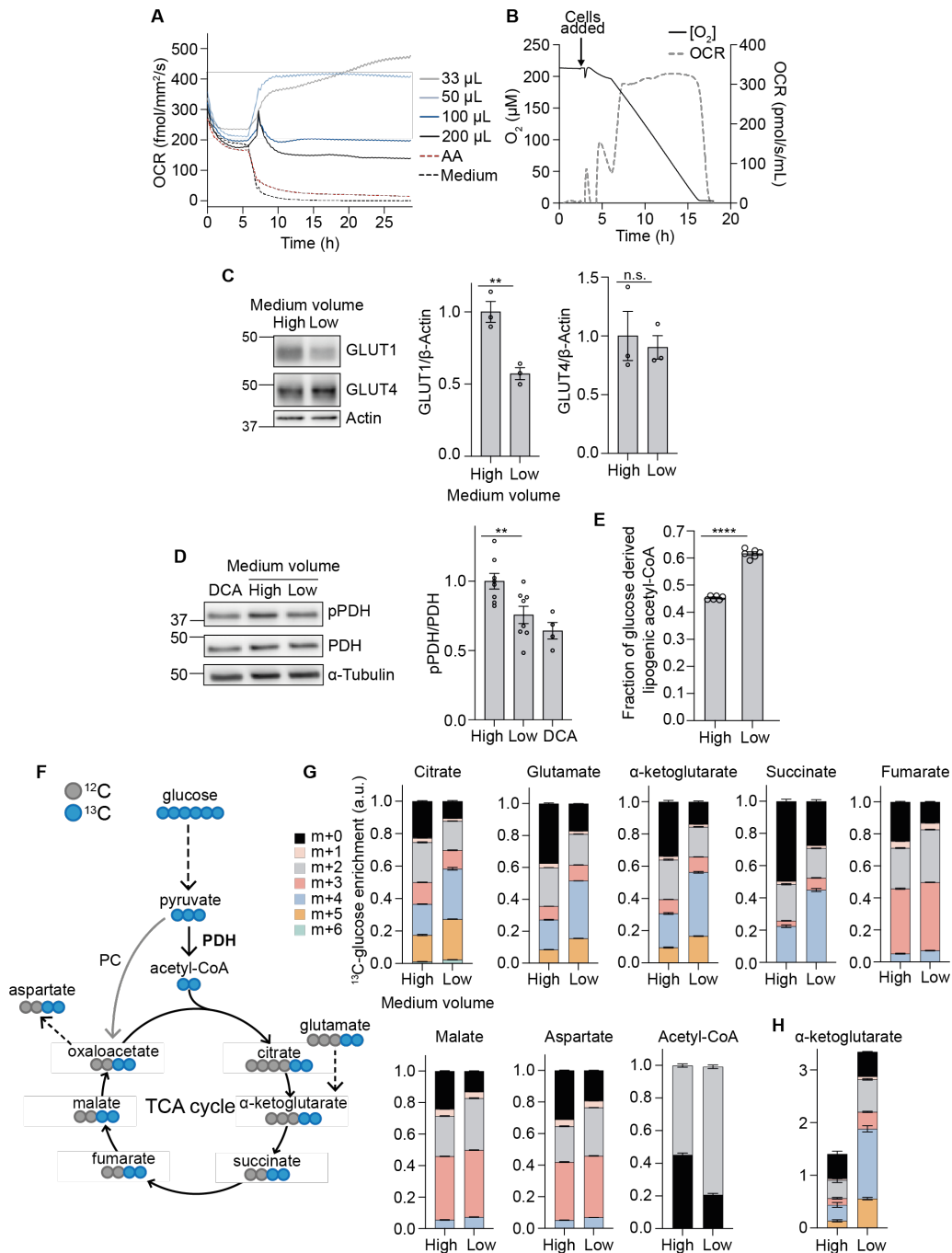
Figure 2. Lowering medium volumes increases mitochondrial glucose oxidation

(A) 3T3-L1 adipocyte oxygen consumption rate (OCR) at different medium volumes, antimycin A (AA) treatment, or medium only conditions. Baseline OCR (at 100 µL medium) was measured for 6 h before altering medium volumes or starting AA and medium only treatments (n = 3 biological replicates).

(B) Oroboros measurements showing oxygen concentration and rate of oxygen consumption (OCR) of 3T3-L1 adipocytes in a closed system (n = 3 biological replicates).

(C) Western blot and quantification of GLUT1 and GLUT4 after 16 h of medium volume change (n = 3 biological replicates).

(D) Western blot and quantification of phospho-pyruvate dehydrogenase (pPDH) and total PDH after 16 h of medium volume change, with dichloroacetate (DCA) as a positive control (n = 8 biological replicates).

(E) Fraction of newly synthesised lipids after 16 h of medium volume change and U^{13}C-glucose labelling (n = 6 biological replicates).

(F) Schematic of ^{13}C enrichment in TCA cycle metabolites after one cycle of U^{13}C-glucose labelling.

(G) Graphs show the fractional abundance of each isotopologue after 16 h medium volume change (n = 6 biological replicates). PC, pyruvate carboxylase.

(H) Total abundance of α-ketoglutarate after 16 h medium volume change (n = 6 biological replicates).

Data are represented as mean ± SEM. n.s., non-significant; **$p < 0.01$, ****$p < 0.0001$ by paired two-tailed Student's t-test (C and D).

See also Figure S2.
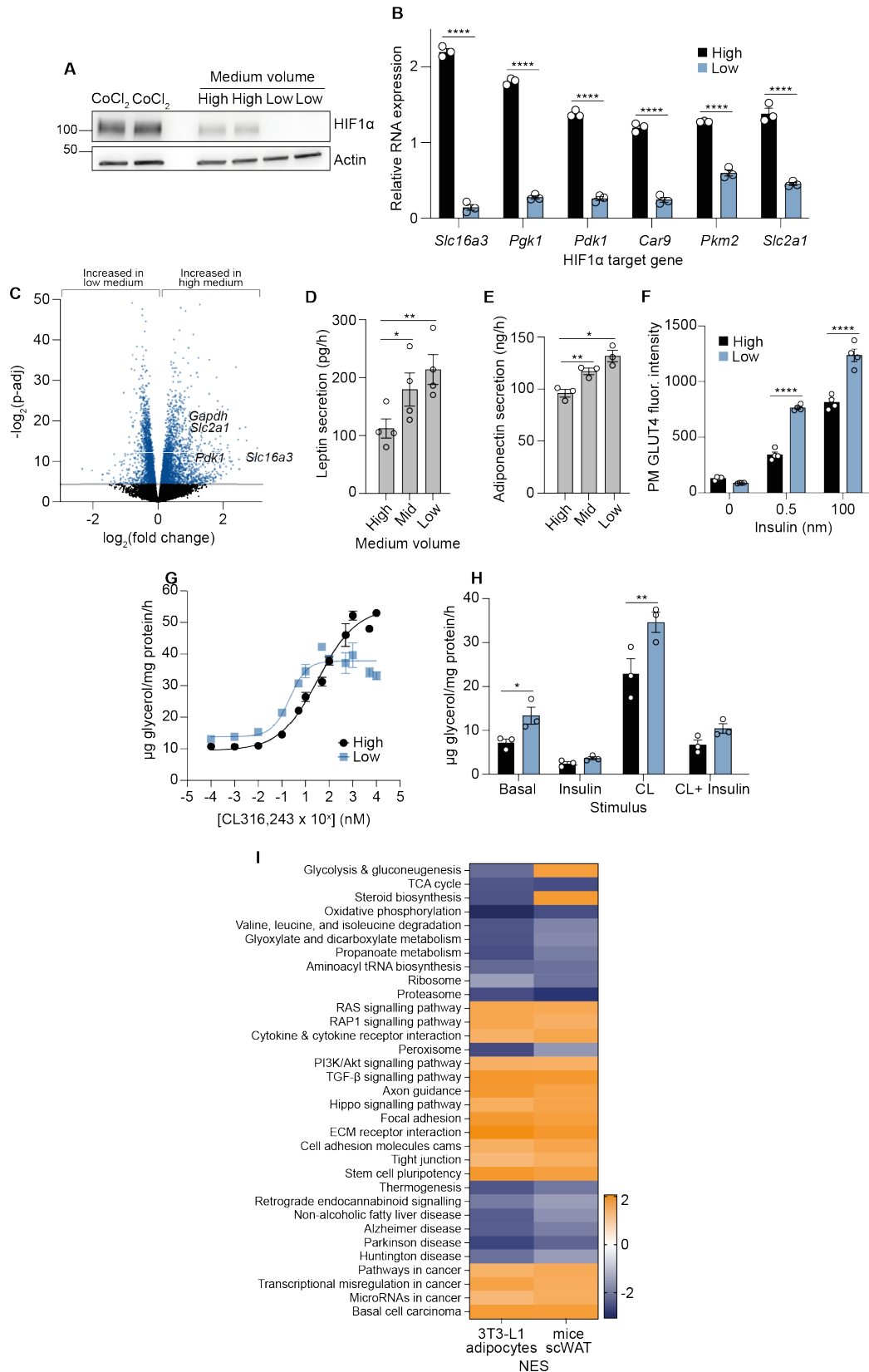
Figure 3. Lowering medium volumes induces a widespread transcriptional response and improves adipocyte function

(A) Western blot of hypoxia-inducible factor (HIF) 1α after 16 h medium volume change, with 500 μM CoCl$_2$ as positive control (n = 3 biological replicates).

(B) Relative RNA expression of HIF1α target genes in 3T3-L1 adipocytes after 16 h medium volume change (n = 3 biological replicates).

(C) Volcano plot of differentially expressed genes after 16 h medium volume change (n = 6 biological replicates).

(D) Rate of leptin secretion under different medium volume conditions (n = 4 biological replicates).

(E) Rate of adiponectin secretion under different medium volume conditions (n = 4 biological replicates).

(F) Fluorescence intensity of plasma membrane (PM) GLUT4 upon insulin stimulation after 48 h medium volume change (n = 4 biological replicates).

(G) Dose response curve of lipolytic drug, CL316,243 treatment (n = 7 biological replicates).

(H) Rate of lipolysis measured by glycerol release, upon 100 nM insulin or 1 nM CL316,243 stimulation (n = 4 biological replicates).

(I) KEGG pathway analyses of 3T3-L1 adipocytes after 16 h medium volume change (n = 6 biological replicates) and subcutaneous white adipose tissue (scWAT) from mice kept in 10% or 21% oxygen for 4 weeks (n = 10 biological replicates). Orange (positive NES) represents upregulated KEGG pathways in high medium (3T3-L1 adipocytes) or in 10% oxygen (mice scWAT). Blue (negative NES) represents upregulated KEGG pathways in low medium (3T3-L1 adipocytes) or in 21% oxygen (mice scWAT). NES, normalised enrichment score.

Data are represented as mean ± SEM. *$p < 0.05$, **$p < 0.01$, ***$p < 0.001$, ****$p < 0.0001$ by one/two-way ANOVA with Šidák correction for multiple comparisons (D, E, F, and H), or by paired Student's t-tests (B).

See also Figure S3.
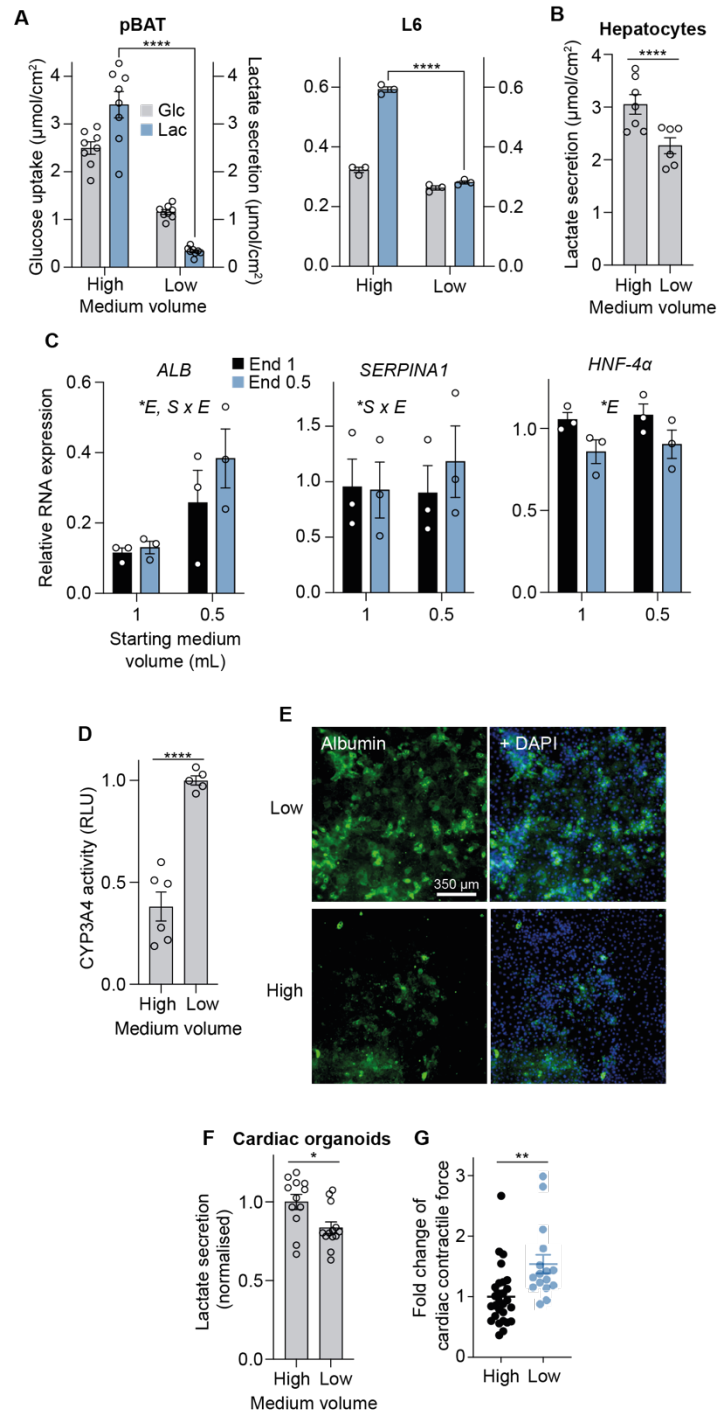
Figure 4. Lowering medium volumes reduces lactate production and improves functional outcomes in other cell types and organoids

(A) Extracellular medium glucose and lactate measurements after 16 h medium volume change in murine brown adipocytes (pBAT) (n = 8 biological replicates) and L6 myotubes (n = 3 biological replicates).

(B) Lactate secretion in iPSC-derived hepatocytes (High = 1 mL, Low = 0.5 mL) after 24 h of medium volume change (n = 7 biological replicates).

(C) Relative RNA expression of hepatocyte differentiation marker genes. Cells were cultured in either 1 mL or 0.5 mL of medium throughout differentiation, and switched to either 1 mL or 0.5 mL of medium 24 h prior to the experiment (n = 3 biological replicates). *E = significance due to end medium volume, *S = significance due to starting medium volume, *S x E = significance due to interaction between starting and end media volumes.

(D) Relative CYP3A4 activity in iPSC-derived hepatocytes after 24 h of medium volume change (n = 6 biological replicates). High = 1 mL, Low = 0.5 mL.

(E) Immunofluorescence of albumin in iPSC-derived hepatocytes after 24 h of medium volume change (n = 3 biological replicates). Scale bar = 350 μm.

(F) Lactate secretion in cardiac organoids after 48 h of medium volume change (normalised) (n = 3-6 technical replicates from n = 3 biological replicates). High = 150 μL, Low = 50 μL.

(G) Cardiac contractile force (normalised) (n = 2-17 technical replicates from n = 4 biological replicates).

All data are represented as mean ± SEM. *$p < 0.05$, **$p < 0.01$, ***$p < 0.001$, ****$p < 0.0001$ by two-way ANOVA with Šidák correction for multiple comparisons (A, C, and F) or by paired/unpaired two-tailed Student's t-test. (B, D, G, and H).

See also Figure S4.

METHODS AND MATERIALS

Cell culture of 3T3-L1 adipocytes

3T3-L1 fibroblasts were cultured in high glucose DMEM supplemented with 10% foetal bovine serum (FBS) and 2 mM glutamax at 37°C in 10% CO_2. For differentiation into adipocytes, fibroblasts were cultured in 10% FBS-supplemented DMEM containing an adipogenic cocktail (350 nM insulin, 0.5 mM 3-isobutyl-1-methylxanthine, and 250 nM dexamethasone for 3 d, followed by 3 d in DMEM containing 10% FBS and 350 nM insulin. Differentiated adipocytes were maintained in 10% FBS-supplemented DMEM. Adipocytes were used for experiments 9–10 d after the onset of differentiation, with culture medium renewed every 2 days prior to each experiment. For low medium volume treatments, cells were cultured in either 1000 µL (high), 666 µL (mid), 333 µL (low) medium in a 12-well plate, or 500 µL (high), 333 µL (mid), or 167 µL (low) in a 24-well plate (Fig S1A) for the duration specific to each experiment.

Measurement of extracellular glucose and lactate concentrations

3T3-L1 adipocytes, pBAT, and L6 myotubes were fed with 1 mL (high), 0.67 mL (mid), or 0.33 mL (low) of fresh medium for 16 h. iPSC-derived hepatocytes were fed with 1 mL (high) or 0.5 mL (low) of fresh medium for 24 h. hPSC-derived cardiac organoids were fed with 150 µL (high) or 50 µL (low) of fresh medium for 48 h. Following low medium volume interventions, media was collected from wells and sent for glucose consumption/lactate production analysis at the Core Biochemical Assay Laboratory (Addenbrooke's Hospital, Cambridge). Naïve medium was used as a baseline. Medium glucose was measured using an adaption of the hexokinase-glucose-6-phosphate dehydrogenase method described by Kunst et al. (1983)[46] (Siemens Healthcare (product code DF30)). Medium lactate was measured by monitoring absorbance at 340 nm due to NADH production as L-lactate is oxidised to pyruvate by lactate dehydrogenase (Siemens Healthcare (product code DF16)). Calculated glucose use and lactate production were normalised to well areas (except in the case of cardiac organoids). Medium lactate from the cardiac organoids were measured using an in-house enzymatic assay, based on the hydrazine-sink method as described previously[8]. Cardiac data were normalised to account for data variability between batches.

Measurements of pericellular oxygen concentration and oxygen consumption rate

3T3-L1 adipocytes were cultured in Falcon flat-bottom 96-well microplate (Corning #353072) with 100 µL medium throughout differentiation. Oxygen consumption rates (OCR) and oxygen concentration were continuously measured using Resipher (Lucid Scientific) at 37°C, 10% CO_2 over 2-3 days starting from 8 d post-differentiation. The Resipher oxygen sensing lid contains micro probes with optical oxygen sensors that scan between 0.55–0.95 mm above the cells to measure the oxygen concentration gradient within the medium column. Baseline OCR and oxygen concentrations under 100 µL medium were measured for 4-6 h in each well. Then, medium volumes were changed and replenished every 24 h. 100 nM antimycin A treatment and trypsinised cells for medium-only wells were used as controls. Data were analysed using the Resipher web application.

Relative measurements of pericellular oxygen concentration

3T3-L1 cells were differentiated in 96-well OxoPlates (PreSens), which have optical oxygen sensors integrated at the bottom of each well. Prior to starting the experiment, different volumes of fresh medium were added to each well, and the plate immediately placed into the plate reader set to 37°C, 10% CO_2 for 24 h. The filters were set up and oxygen levels calculated according to the manufacturer's protocol. Relative oxygen levels were normalised to the 100 µL condition.

3T3-L1 culture in gas-permeable (Lumox) plates

Differentiated 3T3-L1 cells were reseeded on day 6 post-differentiation into 24-well plates (control), or 24-well Lumox plates (Sarstedt), which consist of a black polystyrene frame with a transparent base made from a thin (50 µm), gas-permeable film. The medium volume was

kept at 500 µL throughout the differentiation protocol. At day 9 post-differentiation, 500 µL fresh medium was added and collected after 16 h for glucose and lactate quantification, or cells were scraped for lipid extraction as detailed in the other sections.

Deuterium tracing and lipid extraction

Prior to lipid extraction, cells were cultured in DMEM containing 8% ^{2}H (deuterium)- labelled water, in a 37ºC, 10% CO_2 incubator containing 8% ^{2}H-labelled water for 16 h. Cells were detached with 100 µL ice-cold PBS and lipids extracted and derivatised as fatty acid methyl esters (FAMEs). Lipids were extracted according to a modified Folch method[47] using 50 µM tridecanoic-d25 acid (Cambridge Isotope Laboratories, Inc.) as an internal standard. 1 mL of HPLC-grade chloroform/methanol) 2:1 v/v mixture was added to cell samples in a glass vial. Samples were homogenised by vortexing for 5 min. 200 µL H_2O was added to each sample before vortexing again for 5 min and centrifuging at 4000 x g for 10 min. 600 µL of the lower lipid fraction was transferred to a 7 mL glass tube. A second extraction was performed by adding 600 µL fresh chloroform followed by vortexing and centrifugation as above. Another 600 µL of lower lipid fraction was collected and pooled with the first 600 µL fraction (total = 1200 µL). The collected organic fraction was dried under nitrogen steam and stored at - 80ºC for subsequent gas chromatography-mass spectrometry (GC-MS) analysis.

Fatty acid methyl ester derivatisation and GC-MS analysis

Dried lipids were dissolved in a mixture of 410 µL methanol, 375 µL chloroform, and 90 µL 14% BF_3 for the FAMEs, and incubated at 80ºC for 90 min. 500 µL H_2O and 1000 µL hexane were then added to each sample, homogenised by vortexing briefly, and centrifuged at 2000 rpm for 5 min at room temperature. The organic upper layer was then transferred to an autosampler vial for GC-MS analysis.

GC-MS was performed with Agilent 7890B gas chromatography system linked to Agilent 5977A mass spectrometer, using AS3000 autosampler and data was acquired using MassHunter Workstation Software. A TR-FAME column (length: 30 m, inter diameter: 0.25 mm, film size: 0.25 µm, 260M142P, Thermofisher Scientific) was used with helium as carrier gas. Inlet temperature was set at 230°C. Dried FAME samples were re-suspended in 200 µL HPLC-grade n-Hexane. 1 µl of this solution was injected for analysis. The oven programme used for separation was as follows: 100°C hold for 2 min, ramp at 25°C/min to 150°C, ramp at 2.5°C/min to 162°C and hold for 3.8 min, ramp at 4.5°C/min to 173°C and hold for 5 min, ramp at 5°C/min to 210°C, ramp at 40°C/min to 230°C and hold for 0.5 min. Carrier gas flow was set to constant 1.5 mL/min. If the height of any FAME peaks exceeded 108 units, sample was re-injected with 10:1 – 100:1 split ratio. Identification of FAME peaks was based on retention time and made by comparison with those in external standards (Food industry FAME mix, 35077, Restek).

Peak integration and quantification were performed using MassHunter Workstation Quantitative Analysis software (version B.07.00, Agilent). Specific high-abundance ions from total ion chromatograms were chosen to calculate each fatty acid peak.

Mass isotopomer distribution analysis (MIDA)

To calculate *de novo* lipogenesis rates from fatty acids, MIDA was performed according to the following protocol. In order to perform the analyses we extracted the M+0 to M+4 ions (e.g. for palmitate methyl ester 12 (m/z 270-274)). From these we calculated the fractional concentration of each ion. All equations below use fractional concentrations.

We determined a theoretical distribution for a newly synthesised molecule that was dependent on the precursor labelling pool p, whereby p was the fraction of deuterated water (i.e. 0.08). Firstly, we calculated the isotopomer pattern of each fatty acid caused by the presence of additional 2H atoms in the molecule. The number of available sites in a fatty acid that could

be deuterated, N, was determined based on model fit (e.g. for palmitate in 3T3-L1 adipocytes, N = 14).

Ions dependent on deuterium incorporation were called M'. For each ion M'0-M'4 the following equation gave the expected relative abundance:

For M'x:
(14!/x!*(14-x!)) * px * (1-p)(14-x)

The pattern of labelling based on deuterium was then corrected for the presence of naturally occurring oxygen and carbon isotopes using the following equations for ions M0n-M4n, where Mxn stood for the ion of a newly synthesised fatty acid molecule:

M' = labelling due to deuterium
M = natural isotopic labelling

M0n = M'0*M0
M1n = M'0*M1+M'1*M0
M2n = M'0*M2 + M'1*M1 + M'2*M0
M3n = M'0*M3 + M'1*M2 + M'2*M1 + M'3*M0
M4n = M'0*M4 + M'1*M3 + M'2*M2 + M'3*M1 + M'4*M0

These equations provided us with the ion pattern for a newly synthesised fatty acid M0n-M4n.

To determine the relative contribution of newly synthesised fatty acids and existing fatty acids within the cell we set the following equations, where M0n is newly synthesised, M0 was endogenous pre-existing fatty acids and M0obs was the observed M0 fractional 13 concentration of the ion measured using the mass spectrometer. M0obs' was the calculated fraction of M0 based on combining newly synthesised and pre-existing fatty acid as follows:

M0obs' = f*M0n + (1-f)*M0
M1obs' = f*M1n + (1-f)*M1
M2obs' = f*M2n + (1-f)*M2
M3obs' = f*M3n + (1-f)*M3
M4obs' = f*M4n + (1-f)*M4

We then calculated M0obs-M0obs' through to M4obs-M4obs' and calculated the sum of squares for these 4 equations. We used the GRG Non-Linear Engine of the Solver function of excel to minimise the sum of squares of M0obs-M0obs'+…M4obs-M4obs' by changing the values of p and f. This enabled us to calculate the fractional synthesis rate for each fatty acid. The N number was adjusted until the p was 0.08 (8% deuterated water) which was experimentally set, thus providing the N number. The amount of newly synthesised palmitate was calculated by multiplying the f value by the concentration of the fatty acid in the well.

Measurements of oxygen consumption rate in a closed system
High-resolution O_2 consumption measurements were conducted using the Oroboros Oxygraph-2K (Oroboros Instruments, Innsbruck, Austria) in intact and digitonin-permeabilised cells. For cell experiment, cells were centrifuged at 300 x g for 7 min at room-temperature, washed in PBS, centrifuged once more and then suspended in assay medium at a cell concentration of ~1 x 10^6 viable cells/mL. For experiments designed to assess basal respiratory kinetics in intact cells, differentiated 3T3-L1 adipocytes were suspended in

bicarbonate-free DMEM, supplemented with Glutamax (glucose 4.5 g/L). Respiration and oxygen tension were continuously evaluated until the cells consumed all the available oxygen. For experiments in permeabilized cells, intact 3T3-L1 adipocytes, exposed to low or high medium for 16 h, were suspended in respiration buffer. Respiration buffer consisted of potassium-MES (105 mM; pH 7.2), KCl (30 mM), KH_2PO_4 (10 mM), $MgCl_2$ (5 mM), EGTA (1 mM), and BSA (2.5 g/L). Following basal respiration, cells were permeabilised with digitonin (0.02 mg/mL). Physiological ATP free energy (-54.16 kJ/mol) was applied via the creatine kinase (CK) clamp[48]. Cytochrome *c* (0.01 mM) was added to assess the integrity of the outer mitochondrial membrane, followed by sequential additions of carbon substrates and respiratory inhibitors [pyruvate/malate (Pyr/Mal 5mM/1mM); Glutamate (10 mM); octanoyl-carnitine (Oct 0.2 mM); rotenone (Rot 0.5 µM); Succinate (10 mM); Malonate (10 mM); Calcium (0.6 µM); glycerol-3-phosphate (G3P 10 mM); Antimycin (0.5 µM)]. Data were normalised to total protein.

Immunoblotting

Cells were washed three times in ice-cold PBS and lysed in RIPA buffer containing protease and phosphatase Inhibitors (ThermoFisher). Scraped lysates were then sonicated and centrifuged at 16,000 x g at 4 ºC for 30 min. Protein concentration of the supernatant was quantified using the BCA Assay (Thermo Scientific). Lysates were diluted in 4x Laemmli Sample Buffer (Bio-Rad), reduced with TCEP (ThermoFisher) and heated at 37ºC for 30 min (Figures 2C and S2A; GLUT1, GLUT4, mitochondrial respiratory complexes), or 65ºC for 10 min (Figure 2D; pPDH, PDH). 10-20 µg of protein was resolved by SDS-PAGE and transferred to nitrocellulose membranes (Bio-Rad). Membranes were blocked in 5% skim milk powder in Tris-buffered saline for 1 h at room temperature, followed by an overnight incubation at 4°C with specific primary antibody solutions. Subsequently, membranes were incubated with the appropriate secondary antibodies for 1 h at room temperature before signals were detected using enhanced chemiluminescence (ECL) (Thermo Scientific) on the Chemidoc MP (Bio-Rad). pPDH (1:2000, #31866 Cell Signaling Technology), PDH (1:2000, #2784 Cell Signaling Technology), GLUT4 (1:1000, a gift from F. Koumanov, University of Bath and affinity-purified in-house), GLUT1 (1:1000, #12939 Cell Signaling Technology), α-tubulin (1:1000, #T9026 Sigma Aldrich), OxPhos Rodent WB Antibody Cocktail (1:250, #45-8099 Invitrogen) and β-actin (1:1000, #8457 Cell Signaling Technology) antibodies were used.

Immunoblotting of HIF1α

Cells were washed three times in ice-cold PBS and lysed in 2% SDS containing protease and phosphatase Inhibitors (ThermoFisher), 500 µM $CoCl_2$, and 10 µM MG132. Scraped lysates were then sonicated and centrifuged at 16,000 x g at room temperature for 30 min. Protein concentration of the supernatant was quantified using the BCA Assay (Thermo Scientific). Lysates were diluted in 4x Laemmli Sample Buffer (Bio-Rad), reduced with TCEP (ThermoFisher) and heated at 95ºC for 10 min. 40 µg of protein was resolved by SDS-PAGE and transferred to nitrocellulose membranes (Bio-Rad). Membranes were blocked in 5% skim milk powder in Tris-buffered saline for 1 h at room temperature, followed by an overnight incubation at 4°C with anti-HIF1α (1:500, #14179 Cell Signaling Technology). Subsequently, membranes were incubated with the goat anti-rabbit IgG for 1 h at room temperature before signals were detected using ECL (Thermo Scientific) on the Chemidoc MP (Bio-Rad).

Assessment of PDH flux

PDH flux was assessed using the FASA package implemented in Matlab[49]. FASA was performed on isotope corrected isotopomer distributions for palmitate (M0-M16). Isotope correction was performed using the IsoCorR package implemented in R. The value "D" from the FASA analysis was the proportion of lipogenic acetyl-CoA derived from glucose that was used to produce palmitate.

13C-glucose tracing and metabolite extraction

Prior to the experiment, 3T3-L1 adipocytes were washed once with glucose-free DMEM and labelled with 25 mM 13C-glucose in DMEM for either 4 h or 16 h. Then, medium was removed from the wells and cells were washed twice with room temperature PBS and placed on dry ice. 250 µL metabolite extraction buffer (50% methanol, 30% acetonitrile, 20% ultrapure water, 5 µM valine-d8) was added to each well of a 12-well plate and incubated for 5 min on a dry ice-methanol bath to lyse the cell membranes. After that, extracts were scraped and mixed at 4ºC for 15 min in a thermomixer at 2000 rpm. After final centrifugation at max speed for 20 min at 4ºC, 80 µL of the supernatant from each sample was transferred into labelled LC-MS vials.

LC-MS analysis
Hydrophilic separation of metabolites was achieved using a Millipore Sequant ZIC-pHILIC analytical column (5 µm, 2.1 × 150 mm) equipped with a 2.1 × 20 mm guard column (both 5 mm particle size) with a binary solvent system. Solvent A was 20 mM ammonium carbonate, 0.05% ammonium hydroxide; Solvent B was acetonitrile. The column oven and autosampler tray were held at 40 °C and 4 °C, respectively. The chromatographic gradient was run at a flow rate of 0.200 mL/min as follows: 0–2 min: 80% B; 2-17 min: linear gradient from 80% B to 20% B; 17-17.1 min: linear gradient from 20% B to 80% B; 17.1-23 min: hold at 80% B. Samples were randomised and the injection volume was 5 µl. A pooled quality control (QC) sample was generated from an equal mixture of all individual samples and analysed interspersed at regular intervals.

Metabolites were measured with Vanquish Horizon UHPLC coupled to an Orbitrap Exploris 240 mass spectrometer (both Thermo Fisher Scientific) via a heated electrospray ionisation source. The spray voltages were set to +3.5kV/-2.8 kV, RF lens value at 70, the heated capillary held at 320 °C, and the auxiliary gas heater held at 280 °C. The flow rate for sheath gas, aux gas and sweep gas were set to 40, 15 and 0, respectively. For MS1 scans, mass range was set to m/z=70-900, AGC target set to standard and maximum injection time (IT) set to auto. Data acquisition for experimental samples used full scan mode with polarity switching at an Orbitrap resolution of 120000. Data acquisition for untargeted metabolite identification was performed using the AcquireX Deep Scan workflow, an iterative data-dependent acquisition (DDA) strategy using multiple injections of the pooled sample. DDA full scan-ddMS2 method for AcquireX workflow used the following parameters: full scan resolution was set to 60000, fragmentation resolution to 30000, fragmentation intensity threshold to 5.0e3. Dynamic exclusion was enabled after 1 time and exclusion duration was 10s. Mass tolerance was set to 5ppm. Isolation window was set to 1.2 m/z. Normalised HCD collision energies were set to stepped mode with values at 30, 50, 150. Fragmentation scan range was set to auto, AGC target at standard and max IT at auto. Mild trapping was enabled.

Metabolite identification was performed in the Compound Discoverer software (v 3.2, Thermo Fisher Scientific). Metabolite identities were confirmed using the following parameters: (1) precursor ion m/z was matched within 5 ppm of theoretical mass predicted by the chemical formula; (2) fragment ions were matched within 5 pm to an in-house spectral library of authentic compound standards analysed with the same ddMS2 method with a best match score of over 70; (3) the retention time of metabolites was within 5% of the retention time of a purified standard run with the same chromatographic method. Chromatogram review and peak area integration were performed using the Tracefinder software (v 5.0, Thermo Fisher Scientific) and the peak area for each detected metabolite was normalised against the total ion count (TIC) of that sample to correct any variations introduced from sample handling to instrument analysis. The normalised areas were used as variables for further statistical data analysis.

For $^{13}C_6$-glucose tracing analysis, the theoretical masses of ^{13}C-labelled isotopes were calculated and added to a library of predicted isotopes in Tracefinder 5.0. These masses were then searched with a 5-ppm tolerance and integrated only if the peak apex showed less than 1% deviation in retention time from the [U-^{12}C] monoisotopic mass in the same chromatogram.

The raw data obtained for each isotopologue were then corrected for natural isotope abundances using the AccuCor algorithm (https://github.com/lparsons/accucor) before further statistical analysis.

^{3}H-2-deoxyglucose uptake measurements

3T3-L1 adipocytes were differentiated in 24-well plates with 500 μL medium throughout differentiation. 48 h prior to the assay, medium volumes were changed to either 500 μL (high) or 167 μL (low). On the day of the assay, cells were serum-starved for 2 h with either 500 or 167 μL DMEM containing 0.2% BSA at 37°C, 10% CO_2. Following 2 h serum-starvation, cells were washed and incubated in pre-warmed Krebs–Ringer phosphate (KRP) buffer containing 0.2% bovine serum albumin (BSA, Bovostar, Bovogen) (KRP buffer; 0.6 mM Na_2HPO_4, 0.4 mM NaH_2PO_4, 120 mM NaCl, 6 mM KCl, 1 mM $CaCl_2$, 1.2 mM $MgSO_4$ and 12.5 mM Hepes (pH 7.4)) for 10 min. Again, KRP volumes were maintained at either 500 or 167 μL, and 200 μM indinavir[50] was added to at this point where indicated. Adipocytes were then stimulated with 100 nM insulin for 20 min. To determine non-specific glucose uptake, 25 μM cytochalasin B (in ethanol, Sigma Aldrich) was added to control wells before addition of 2-[^{3}H]deoxyglucose (2-DG) (PerkinElmer). During the final 5 min 2-DG (0.25 μCi, 50 μM) was added to cells to measure steady-state rates of 2-DG uptake. Note that the volumes of 2-DG added were altered to account for different medium volumes. Cells were then moved to ice, washed with ice-cold PBS, and solubilised in PBS containing 1% (v/v) Triton X-100. Tracer uptake was quantified by liquid scintillation counting and data normalised for protein content.

qRT-PCR

3T3-L1 adipocytes were cultured using 1 mL medium (12-well plate) throughout differentiation. Medium volumes were changed to either 1 mL or 0.33 mL 16 h prior to the assay. Hepatocytes were cultured in either 1 mL or 0.5 mL medium (12-well plate) throughout differentiation, and changed to either 1 mL or 0.5 mL 24 h prior to the assay. RNA extractions were performed using the RNeasy Mini kit (Qiagen 1152 #74104). Concentrations of RNA samples were quantified using NanoDrop. cDNA synthesis from 500 ng RNA was performed using the GoScript Reverse Transcriptase kit (Promega #A2801). Real-time (RT)-polymerase chain reaction (PCR) was performed with SYBR Green Master Mix on the ABI QuantStudio 5.

Subcutaneous white adipose tissue (scWAT) from normoxic and hypoxic mice

Animal work was carried out in accordance with United Kingdom Home Office regulations under the Animals in Scientific Procedures (1986) Act and underwent review by the University of Cambridge Animal Welfare and Ethical Review Board. All procedures involving live animals were carried out by a personal licence holder in accordance with these regulations.

Subcutaneous adipose tissue (scWAT) was collected from mice exposed to either 10% O_2 or maintained under normoxic atmospheric conditions, from a larger experimental cohort as previously published[51,52]. 129Ev/Sv mice were housed in conventional cages from birth in a temperature- (23°C) and humidity-controlled environment with a 12 h photoperiod and given *ad libitum* access to standard rodent chow (RM1(E), Special Diet Services, UK) and water. At 7 weeks of age, mice were randomly assigned to remain under normoxic conditions, or transferred to a normobaric hypoxia chamber (10% O_2; PFI systems, Milton Keynes, UK). Mice were maintained in hypoxia or normoxia for 28 days, after which they were killed by cervical dislocation. The scWAT was removed from the inguinal region, snap frozen and stored at -80°C until further analysis. The inguinal lymph node was removed from scWAT depots prior to RNA-seq analysis.

RNA extraction and sequencing

3T3-L1 adipocytes were seeded and differentiated in 12-well plates. RNA extraction from adipocytes was performed using the RNeasy Mini Kit (Qiagen 1152 #74104).

RNA extraction from mice scWAT was performed by homogenisation in RNA STAT-60. Samples were broken up using a pestle and mortar under liquid nitrogen. The broken pieces were then put in 2 mL screw-top tubes with Lysing Matrix D (MP Biomedicals). 1 mL STAT-60 was added to the tissue samples, followed by homogenisation using Precellys 24 Touch. The homogenate was then transferred to 1.5 mL eppendorfs. Tubes were spun at 13,000 rpm for 5 min at 4°C to remove debris. The supernatant was removed and transferred to fresh tubes containing 200 µL of Chloroform. Samples were vortexed at maximum speed for 15 s, and spun at 12,000 g for 15 min at 4°C. A clear aqueous supernatant of around 600 µL for every 1 mL of STAT-60 added will have formed. The aqueous phase was transferred to fresh tubes containing 500 µL of isopropanol. Tubes were mixed by inversion several times and left at -20°C overnight. After overnight incubation, the precipitates were spun at 12,000 g for 10 min at 4°C to pellet RNA. After removing the supernatant, 1 mL of cold 70% ethanol (stored at -20°C) was added to the pellet and washed by vortexing briefly. Samples were then spun at 8000 g for 5 min at 4°C before discarding the supernatant. Pellets were air-dried for 10-15 min on ice until transparent. Nuclease-free water was added to the pellet and incubated at 60°C for 10 min. Samples were placed on ice and re-suspended by pipetting up and down.

RNA samples from both 3T3-L1 adipocytes and mice scWAT were quantified using nanodrop. 1 µg of total RNA was quality checked (RIN >7) using an Agilent Bioanalyser 2100 system and then used to construct barcoded sequencing libraries with Illumina's TruSeq Stranded mRNA Library Prep Kit following manufacturer's instruction. All the libraries were then multiplexed and sequenced on one lane of Illumina NovaSeq6000 at PE50 at the CRUK Cambridge Institute Genomics Core Facility.

RNAseq data analysis

The NGS data were processed through a customised pipeline. FastQC software (v. 0.11.9) was used for generating quality-control reports of individual FASTQ files (http://www.bioinformatics.babraham.ac.uk/projects/fastqc). RNA sequencing reads were aligned to the *mus musculus* (mouse) GRCm38 genome using hisat2 (v2.1.0)[53]. HTseq-count (v 0.11.1)[54] was then used for gene counting and DESeq2 (v3.15)[55] for differential gene expression analysis (Wald Test). The raw p values were adjusted by the Benjamini-Hochberg procedure to control the False Discovery Rate (FDR). Pathway enrichment analysis was performed with FGSEA (fast gene set enrichment analysis)[56] using pre-ranked gene lists and pathways from the KEGG database[57,58].

For the inference of the upstream transcriptional regulators we used VIPER (Virtual Inference of Protein-activity by Enriched Regulon analysis)[59]. The estimation of their activation/inhibition status is based on the differential expression of their known target genes and is represented by a positive or negative NES (normalised enrichment score), respectively. The network that links the transcriptional regulators with their target genes was derived from DoRothEA (https://saezlab.github.io/dorothea/)[60].

Measurement of extracellular leptin and adiponectin

3T3-L1 adipocytes were cultured as described above. Cells were transferred to low or high medium at the volumes stated above for 48 h, before media was collected and analysed by the Core Biochemical Assay Laboratory (Addenbrooke's Hospital, Cambridge). Leptin concentration was determined using the MesoScale Discovery Mouse Leptin Kit (K152BYC-2, Rockville, MD, USA), and adiponectin concentration using the MesoScale Discovery Mouse Adiponectin Kit (K152BXC, Rockville, MD, USA) according to manufacturer's instructions.

Immunofluorescence analysis of GLUT4 translocation in 3T3-L1 adipocytes

Cells were differentiated in black CellCarrier-96 Ultra Microplates (PerkinElmer). Cells were cultured in specified medium volumes for 48 h prior to assay and medium volumes were kept the same throughout the assay until cells were fixed. Cells were serum-starved in DMEM containing 0.2% BSA for 2 h at 37°C, 10% CO_2, and then stimulated with 0.5 nM or 100 nM

insulin for 20 min. Cells were then washed in an ice-cold PBS bath and instantly fixed with 4% paraformaldehyde on ice for 5 min, followed by 15 min at room temperature. Cells were then quenched with 50 mM glycine for 10 min, then washed twice with PBS at room temperature, and incubated in blocking buffer (5% normal swine serum in PBS) for 20 min. After blocking, cells were incubated with anti-GLUT4 (LM048) (2 µg/mL, Integral Molecular, PA, USA) and Lectin-FITC conjugate (Sigma #L4895) for 1 h at room temperature. This antibody recognises an external epitope on GLUT4, and so staining in non-permeabilised cells will only label GLUT4 present in the plasma membrane[61]. Then, cells were washed in PBS and incubated with anti-human Alexa-647 (1:500, ThermoFisher), and Hoechst 33342 (1:5000) room temperature. After 1 h, the plates were washed three times in PBS, then stored and imaged in PBS, 5% glycerol and 2.5% Dabco. Imaging was performed with the Opera Phenix (Perkin Elmer) using a 20x NA1.0 water immersion objective. Nine fields of view were imaged per well and analysed using a custom pipeline in Harmony High-Content Imaging and Analysis Software (Perkin Elmer). Cell plasma membrane regions were defined using the lectin-FITC signal and the anti-GLUT4 signal within this region calculated as a measure of GLUT4 translocation.

CL dose response and lipolysis assay
3T3-L1 adipocytes were cultured as described above. All lipolysis experiments were performed on day 10 following differentiation. Medium volume interventions were carried out 48 h prior to the experiment, and cells were kept in the appropriate medium volumes (high or low) for the duration of the lipolysis experiments. Cells were serum-starved in DMEM containing 0.2% BSA for 2 h at 37°C, 10% CO_2, and then stimulated with the appropriate agonist (insulin or CL316,243 (Tocris)) in KRP buffer for 30 min at 37°C. Glycerol release into the KRP buffer was determined using the free glycerol reagent (Sigma, #F6428) and absorbance measured at 595 nm. Glycerol release was normalised to cellular protein content (determined by BCA) of cells lysed in PBS containing 1% triton.

Cell culture of iPSC-derived hepatocytes
Human induced pluripotent stem cells (iPSCs) were maintained on vitronectin XFTM (10 µg/mL, StemCell Technologies)-coated plates and in Essential 8 (E8) medium consisting of DMEM/F12 (Gibco), L-ascorbic acid 2-phosphate (1%), insulin-transferrin-selenium solution (2%, Life Technologies), sodium bicarbonate (0.7%), and Penicillin/Streptomycin (P/S) (1%), freshly supplemented with TGFβ (10 ng/mL, R&D) and FGF2 (12 ng/mL, Qkine). Cells were split every 5-7 days by incubation with 0.5 µM EDTA (Thermo Fisher Scientific) for 4 min at room temperature and clumps were dissociated into small clumps by pipetting. For iPSC differentiation, iPSCs were split into single cells using Accutase (StemCell Technologies) and seeded at a density of 50,000 cells per cm^2 in E8 media with 10 µM ROCK Inhibitor Y-27632 (Selleckchem). Cells were differentiated towards hepatocytes as previously described[62] with minor modifications. For foregut specification, cells were incubated for 5 days in RPMI media with 2% B27 and 50 ng/mL Activin (R&D). Cells were differentiated into hepatocytes using HepatoZYME media (Thermo) with 2 mM L-glutamine, 1% P/S, 2% non-essential amino acids (Thermo), 2% chemically defined lipids (Thermo), 30 µg/mL transferrin (Roche), 14 µg/mL insulin (Roche), 20 ng/mL Oncostatin M (R&D) and 50 ng/mL hepatocyte growth factor (R&D). Cells were analysed at day 32 of differentiation. For media volume experiments, cells were differentiated towards hepatocytes in either 0.5 mL or 1 mL of complete HepatoZYME media, and volumes were changed or unchanged for the last 24 h of the experiment.

CYP3A4 activity assay
CYP3A4 enzymatic activity was measured using the P450 Glo kit (Promega). Cells were incubated with 1:1000 luciferin-IPA in Hepatozyme complete for 1 h at 37°C. 50 µL of cell culture supernatant was mixed with 50 µL detection reagent and incubated 20 min at room temperature in Greiner white 96-well microplates (Sigma-Aldrich). Luminescence was measured in triplicate on a GloMax plate reader. Hepatozyme complete medium was used as background control.

Immunofluorescence analysis of albumin in iPSC-derived hepatocytes

Cells were fixed in 4% PFA for 15 min at room temperature, washed 3x in PBS and blocked for 1 h in PBS with 10% donkey serum and 0.1% Triton X-100 for permeabilisation. Anti-albumin antibody (Bethyl Labs #A80-229A) was applied in blocking solution overnight at 4°C. Cells were then washed 3x in PBS and incubated in Alexa Fluor 488-conjugated secondary antibody (Life Technologies) in blocking solution, with 3 µM DAPI for 1 h at room temperature. Cells were then washed 3x in PBS and visualised in the plate using a Zeiss inverted 710 confocal microscope.

hPSC-derived cardiac organoids

Ethical approval for the use of human embryonic stem cells (hPSCs) was obtained from QIMR Berghofer's Ethics Committee (P2385), and was carried out in accordance with the National Health and Medical Research Council of Australia (NHMRC) regulations. Female HES3 (WiCell) were maintained in mTeSR PLUS (Stem Cell Technologies)/ Matrigel (Millipore) and passaged using T ReLeSR (Stem Cell Technologies). Quality control was performed with karyotyping (G-banding) and mycoplasma testing. hPSC-derived cardiac organoids were generated as recently described[63].

Cardiomyocyte and stromal cell differentiation was achieved using previously described protocols[64-67]. hPSCs were seeded on Matrigel-coated flasks at 2×10^4 cells/cm^2 and cultured in mTeSR-1 for 4 days. To induce cardiac mesoderm, hPSCs were cultured in RPMI B27-medium (RPMI 1640 GlutaMAX+ 2% B27 supplement without insulin, 200µM L-ascorbic acid 2-phosphate sesquimagnesium salt hydrate (Sigma) and 1% penicillin/streptomycin (ThermoFisher Scientific), supplemented with 5 ng/ml BMP-4 (RnD Systems), 9 ng/ml Activin A (RnD Systems), 5 ng/ml FGF-2 (RnD Systems) and 1 µM CHIR99021 (Stemgent or Stem Cell Technologies). Mesoderm induction required daily medium exchanges for 3 days. This was followed by cardiac specification using RPMI B27- containing 5 µM IWP-4 (Stem Cell Technologies) for another 3 days, and then further 7 days using 5 µM IWP-4 RPMI B27+ (RPMI1640 Glutamax + 2% B27 supplement with insulin, 200µM L-ascorbic acid 2-phosphate sesquimagnesium salt hydrate and 1% penicillin/streptomycin) with medium change every 2-3 days. For the final 2 days of differentiation, hPSCs were cultured in RPMI B27+. Harvest of differentiated cardiac cells involved enzymatic digestion, firstly in 0.2% collagenase type I (Sigma) in 20% fetal bovine serum (FBS, ThermoFisher Scientific) in PBS (with Ca^{2+} and Mg^{2+}) at 37°C for 1 hour, and secondly in 0.25% trypsin-EDTA at 37°C for 10 minutes. The trypsin was neutralized, and then cells were filtered through a 100 µm mesh cell strainer (BD Biosciences), centrifuged at 300 x g for 3 minutes, and resuspended in α-MEM Glutamax, 10% FBS, 200 µM L-ascorbic acid 2-phosphate sesquimagnesium salt hydrate and 1% penicillin/streptomycin (MEM++++). Previous flow cytometry analysis indicated that differentiated cardiac cells were ~70% α-actinin$^+$/CTNT$^+$ cardiomyocytes, ~30% CD90 stromal cells[66].

hCO culture inserts were fabricated using SU-8 photolithography and PDMS moulding[64]. Acid-solubilized bovine collagen 1 (Devro) was salt balanced using 10x DMEM (ThermoFisher Scientific) and pH neutralised using 0.1M NaOH before combining with Matrigel and then the cell suspension on ice. Each hCO contained 5×10^4 cells, a final concentration of 2.6 mg/ml collagen I and 9% Matrigel. 3.5 µL of suspension was pipetted into the hCO culture insert and incubated at 37°C with 5% CO$_2$ for 45 min in order to gel. After gelling, α-MEM GlutaMAX (ThermoFisher Scientific), 10% foetal bovine serum (FBS), 200 µM L-ascorbic acid 2-phosphate sesquimagnesium salt hydrate (Sigma) and 1% Penicillin/Streptomycin (ThermoFisher Scientific) was added. hCO were subsequently cultured in maturation medium (MM)[64] with medium changes every 2 to 3 days for 5 days (7 days old hCO). To better approximate adult metabolic provisions a 'weaning medium' (WM) was utilised. hCO were cultured in WM containing 4% B27 – insulin, 5.5 mM glucose, 1 nM insulin, 200 µM L-ascorbic acid 2-phosphate sesquimagnesium salt hydrate, 1% P/S, 1% GlutaMAX (100x), 33 µg/mL

aprotinin and 10 μM palmitate (conjugated to bovine serum albumin in B27) in DMEM without glucose, glutamine and phenol red (ThermoFisher Scientific) with medium changes every 2-3 days.

The elasticity of the Heart Dyno poles enables the contractile properties to be determined via tracking pole deflection, which directly correlates with force[64]. Videos of 10 s were made of each hCO with the Nikon ANDOR WD Revolution Spinning Disk microscope (magnification 4x). While imaging, hCO were incubated at 37°C, 5% CO_2 to prevent changes in contractile behaviour. This facilitated the analysis of the contractile properties of the organoids and the production of time-force graphs[64]. Moreover, data was obtained regarding additional important functional parameters including the contraction rate and the activation and relaxation time of the organoids.

Statistical analysis

All statistical analyses, unless otherwise stated in figure legends, were carried out using GraphPad Prism 9. Two-tailed paired/unpaired Student's t-tests were used to compare the means between two groups. One/two-way ANOVA with Šidák correction for multiple comparisons was performed for multigroup (at least three) comparisons. Data are presented as mean ± SEM, of at least three independent biological replicates.

REFERENCES AND NOTES

1. Ast, T., and Mootha, V.K. (2019). Oxygen and mammalian cell culture: are we repeating the experiment of Dr. Ox? Nat. Metab. *9*, 858–860. doi: 10.1038/s42255-019-0105-0; pmid: 32694740

2. Place, T.L., Domann, F.E., and Case, A.J. (2017). Limitations of oxygen delivery to cells in culture: An underappreciated problem in basic and translational research. Free Radic. Biol. Med. *113*, 311–322. doi: 10.1016/j.freeradbiomed; pmid: 29032224

3. McLimans, W.F., Blumenson, L.E., and Tunnah, K.V. (1968). Kinetics of gas diffusion in mammalian cell culture systems. II. Theory. Biotechnol. Bioeng. *10*, 741–763. doi: 10.1002/bit.260100604

4. Jensen, M.D., Wallach, D.F.H., and Sherwood, P. (1976). Diffusion in tissue cultures on gas-permeable and impermeable supports. J. Theor. Biol. *56*, 443–458. doi: 10.1016/s0022-5193(76)80085-9; pmid: 5633

5. Keeley, T.P., and Mann, G.E. (2019). Defining Physiological Normoxia for Improved Translation of Cell Physiology to Animal Models and Humans. Physiol. Rev. *1*, 161–234. doi: 10.1152/physrev.00041.2017; pmid: 30354965

6. Metzen, E., Wolff, M., Fandrey, J., and Jelkmann, W. (1995). Pericellular PO2 and O2 consumption in monolayer cell cultures. Respir. Physiol. *100*, 101–6. doi: 10.1016/0034-5687(94)00125-j; pmid: 7624611

7. Wolff, M., Fandrey, J., and Jelkmann, W. (1993) Microelectrode measurements of pericellular PO2 in erythropoietin-producing human hepatoma cell cultures. Am. J. Physiol. *265*, C1266–70. doi: 10.1152/ajpcell.1993.265.5.C1266; pmid: 8238479

8. Krycer, J.R., Quek, L.E., Francis, D., Fazakerley, D.J., Elkington, S.D., Diaz-Vegas, A., Cooke, K.C., Weiss, F.C., Duan, X., Kurdyukov, S., Zhou, P.X., Tambar, U.K., Hirayama, A., Ikeda, S., Kamei, Y., Soga, T., Cooney, G.J., and James, D.E. (2020). Lactate production is a prioritized feature of adipocyte metabolism. J. Biol. Chem. *295*, 83–98. doi: 10.1074/jbc.RA119.011178; pmid: 31690627

9. Henry, O., Jolicoeur, M., and Kamen, A. (2011) Unraveling the metabolism of HEK-293 cells using lactate isotopomer analysis. Bioprocess Biosyst. Eng. *34*, 263–273. doi: 10.1007/s00449-010-0468-9; pmid: 20848294

10. Gilglioni, E.H., Chang, J.C., Duijst, S., Go, S., Adam, A.A.A., Hoekstra, R., Verhoeven, A.J., Ishii-Iwamoto, E.L., and Oude Elferink, R.P.J. (2018). Improved oxygenation dramatically alters metabolism and gene expression in cultured primary mouse hepatocytes. Hepatol. Commun. *2*, 299–312. doi: 10.1002/hep4.1140; pmid: 29507904

11. Gstraunthaler, G., Seppi, T., and Pfaller, W. (1999). Impact of culture conditions, culture media volumes, and glucose content on metabolic properties of renal epithelial cell cultures. Are renal cells in tissue culture hypoxic? Cell Physiol. Biochem. *9*, 150–172. doi: 10.1159/000016312; pmid: 10494029

12. Han, X., and Simon, M.C. (2022). NAD+ regeneration drives cancer cell proliferation. Nat. Metab. *4*, 647–648. doi: 10.1038/s42255-022-00586-w; pmid: 35739398

13. Arnold, P.K., Jackson, B.T., Paras, K.I., Brunner, J.S., Hart, M.L., Newsom, O.J., Alibeckoff, S.P., Endress, J., Drill, E., Sullivan, L.B., and Finley, L.W.S. (2022). A non-canonical tricarboxylic acid cycle underlies cellular identity. Nature *603*, 477–481. doi: 10.1038/s41586-022-04475-w; pmid: 35264789

14. Liberti, M.V., and Locasale, J.W. (2016). The Warburg Effect: How Does it Benefit Cancer Cells? Trends Biochem. Sci. *41*, 211–218. doi: 10.1016/j.tibs.2015.12.001; pmid: 26778478

15. Luengo, A., Li, Z., Gui, D.Y., Sullivan, L.B., Zagorulya, M., Do, B.T., Ferreira, R., Naamati, A., Ali, A., Lewis, C.A., Thomas, C.J., Spranger, S., Matheson, N.J., and Vander Heiden, M.G. (2021). Increased demand for NAD+ relative to ATP drives aerobic glycolysis. Mol. Cell *81*, 691–707. doi: 10.1016/j.molcel.2020.12.012; pmid: 33382985

16. Crabtree, H.G. (1929). Observations on the carbohydrate metabolism of tumours. Biochem. J. *23*, 536–45. doi: 10.1042/bj0230536; pmid: 16744238

17. Mot, A.I., Liddell, J.R., White, A.R., and Crouch, P.J. (2016). Circumventing the Crabtree Effect: A method to induce lactate consumption and increase oxidative phosphorylation in cell culture. Int. J. Biochem. Cell Biol. *79*, 128–138. doi: 10.1016/j.biocel.2016.08.029; pmid: 27590850

18. Vander Heiden, M.G., Cantley, L.C., and Thompson, C.B. (2009). Understanding the Warburg effect: the metabolic requirements of cell proliferation. Science *324*, 1029–33. doi: 10.1126/science.1160809; pmid: 19460998

19. Green, H., and Kehinde, O. (1975). An established preadipose cell line and its differentiation in culture II. Factors affecting the adipose conversion. Cell *5*, 19–27. doi: 10.1016/0092-8674(75)90087-2; pmid: 165899

20. Fu, M., Sun, T., Bookout, A.L., Downes, M., Yu, R.T., Evans, R.M., and Mangelsdorf, D.J. (2005). A Nuclear Receptor Atlas: 3T3-L1 adipogenesis. Mol. Endocrinol. *19*, 2437–2450. doi: 10.1210/me.2004-0539; pmid: 16051663

21. Chen, Z., Torrens, J.I., Anand, A., Spiegelman, B.M., and Friedman, J.M. (2005). Krox20 stimulates adipogenesis via C/EBPbeta-dependent and -independent mechanisms. Cell Metab. *1*, 93–106. doi: 10.1016/j.cmet.2004.12.009; pmid: 16054051

22. Ren, D., Collingwood, T.N., Rebar, E.J., Wolffe, A.P., and Camp, H.S. (2002). PPARgamma knockdown by engineered transcription factors: exogenous PPARgamma2 but not PPARgamma1 reactivates adipogenesis. Genes Dev. *16*, 27–32. doi: 10.1101/gad.953802; pmid: 11782442

23. Green, C.R., Wallace, M., Divakaruni, A.S., Phillips, S.A., Murphy, A.N., Ciaraldi, T.P., and Metallo, C.M. (2016). Branched-chain amino acid catabolism fuels adipocyte differentiation and lipogenesis. Nat. Chem. Biol. *12*, 15–21. doi: 10.1038/nchembio.1961; pmid: 26571352

24. Tan, S.X., Fisher-Wellman, K.H., Fazakerley, D.J., Ng, Y., Pant, H., Li, J., Meoli, C.C., Coster, A.C., Stöckli, J., and James, D.E. (2015). Selective insulin resistance in adipocytes. J. Biol. Chem. *290*, 11337–11348. doi: 10.1074/jbc.M114.623686; pmid: 25720492

25. Stevens, K.M. (1965). Oxygen requirements for liver cells in vitro. Nature *206*, 199. doi: 10.1038/206199a0; pmid: 5890441

26. Sheng, X., Tucci, J., Malvar, J., and Mittelman, S.D. (2014). Adipocyte differentiation is affected by media height above the cell layer. Int. J. Obes. *38*, 315–320. doi: 10.1038/ijo.2013.96; pmid: 23743593

27. Lehninger, A.L., Nelson, D.L., and Cox, M.M. (1993). Principles of Biochemistry 2 (Worth, New York).

28. Papandreou, I., Cairns, R.A., Fontana, L., Lim, A.L., and Denko, N.C. (2006). HIF-1 mediates adaptation to hypoxia by actively downregulating mitochondrial oxygen consumption. Cell Metab. *3*, 187–197. doi: 10.1016/j.cmet.2006.01.012; pmid: 16517406

29. Kim, J.W., Tchernyshyov, I., Semenza, G.L., and Dang, C.V. (2006). HIF-1-mediated expression of pyruvate dehydrogenase kinase: a metabolic switch required for cellular adaptation to hypoxia. Cell Metab. *3*, 177–85. doi: 10.1016/j.cmet.2006.02.002; pmid: 16517405

30. Dengler, V.L., Galbraith, M., and Espinosa, J.M. (2014). Transcriptional regulation by hypoxia inducible factors. Crit. Rev. Biochem. Mol. Biol. *49*, 1–15. doi: 10.3109/10409238.2013.838205; pmid: 24099156

31. Schofield, C., and Ratcliffe, P. (2004). Oxygen sensing by HIF hydroxylases. Nat. Rev. Mol. Cell. Biol. *5*, 343–354. doi: 10.1038/nrm1366; pmid: 15122348

32. Kolobova, E., Tuganova, A., Boulatnikov, I., and Popov, K.M. (2001). Regulation of pyruvate dehydrogenase activity through phosphorylation at multiple sites. Biochem. J. *15*, 69–77. doi: 10.1042/0264-6021:3580069; pmid: 11485553

33. Hellerstein, M.K., and Neese, R.A. (1992). Mass isotopomer distribution analysis: A technique for measuring biosynthesis and turnover of polymers. Am. J. Physiol. *263*, E988–E1001. doi: 10.1152/ajpendo.1992.263.5.E988; pmid: 1443132

34. Tennant, D., Frezza, C., MacKenzie, E.D., Nguyen, Q.D., Zheng, L., Selak, M.A., Roberts, D.L., Dive, C., Watson, D.G., Aboagye, E.O., and Gottlieb, E. (2009). Reactivating HIF prolyl hydroxylases under hypoxia results in metabolic catastrophe and cell death. Oncogene *28*, 4009–4021. doi: 10.1038/onc.2009.250; pmid: 19718054

35. Iommarini, L., Porcelli, A.M., Gasparre, G., and Kurelac, I. (2017). Non-canonical mechanisms regulating hypoxia-inducible factor 1 alpha in cancer. Front. Oncol. 7, 286. doi: 10.3389/fonc.2017.00286; pmid: 29230384

36. Pan, Y., Mansfield, K.D., Bertozzi, C.C., Rudenko, V., Chan, D.A., Giaccia, A.J., and Simon, M.C. (2007). Multiple factors affecting cellular redox status and energy metabolism modulate hypoxia-inducible factor prolyl hydroxylase activity in vivo and in vitro. Mol. Cell. Biol. *27*, 912–925. doi: 10.1128/MCB.01223-06; pmid: 17101781

37. Chen, C., Pore, N., Behrooz, A., Ismail-Beigi, F., and Maity, A. (2001). Regulation of glut1 mRNA by hypoxia-inducible factor-1. Interaction between H-ras and hypoxia. J. Biol. Chem. *276*, 9519–9525. doi: 10.1074/jbc.M010144200; pmid: 11120745

38. Watt, A.J., Garrison, W.D., and Duncan, S.A. (2003). HNF4: a central regulator of hepatocyte differentiation and function. Hepatology *37*, 1249–1253. doi: 10.1053/jhep.2003.50273; pmid: 12774000

39. DeLaForest, A., Nagaoka, M., Si-Tayeb, K., Noto, F.K., Konopka, G., Battle, M.A., and Duncan, S.A. (2011). HNF4A is essential for specification of hepatic progenitors from human pluripotent stem cells. Development *138*, 4143–4153. doi: 10.1242/dev.062547; pmid: 21852396

40. Gilglioni, E.H., Chang, J.C., Duijst, S., Go, S., Adam, A., Hoekstra, R., Verhoeven, A. J., Ishii-Iwamoto, E.L., and Oude Elferink, R. (2018). Improved oxygenation dramatically alters metabolism and gene expression in cultured primary mouse hepatocytes. Hepatol. Commun. *2*, 299–312. doi: 10.1002/hep4.1140; pmid: 29507904

41. Poyck, P.P., Mareels, G., Hoekstra, R., van Wijk, A.C., van der Hoeven, T.V., van Gulik, T.M. , Verdonck, P.R., and Chamuleau, R.A. (2008). Enhanced oxygen availability improves liver-specific functions of the AMC bioartificial liver. Artificial organs *32*, 116–126. doi: 10.1111/j.1525-1594.2007.00500.x; pmid: 18005273

42. Abo, K.M., Sainz de Aja, J., Lindstrom-Vautrin, J., Alysandratos, K.D., Richards, A., Garcia-de-Alba, C., Huang, J., Hix, O.T., Werder, R.B., Bullitt, E., Hinds, A., Falconer, I., Villacorta-Martin, C., Jaenisch, R., Kim, C.F., Kotton, D.N., Wilson, A.A. (2022). Air-liquid interface culture promotes maturation and allows environmental exposure of pluripotent stem cell-derived alveolar epithelium. JCI Insight *7*, e155589. doi: 10.1172/jci.insight.155589; pmid: 35315362

43. Giandomenico, S.L., Mierau, S.B., Gibbons, G.M., Wenger, L.M.D., Masullo, L., Sit, T., Sutcliffe, M., Boulanger, J., Tripodi, M., Derivery, E., Paulsen, O., Lakatos, A., Lancaster, M.A. (2019). Cerebral organoids at the air-liquid interface generate diverse nerve tracts with functional output. Nat. Neurosci. *22*, 669–679. doi: 10.1038/s41593-019-0350-2; pmid: 30886407

44. Neal, J.T., Li, X., Zhu, J., Giangarra, V., Grzeskowiak, C.L., Ju, J., Liu, I.H., Chiou, S.H., Salahudeen, A.A., Smith, A.R., Deutsch, B.C., Liao, L., Zemek, A.J., Zhao, F., Karlsson, K., Schultz, L.M., Metzner, T.J., Nadauld, L.D., Tseng, Y.Y., Alkhairy, S., Oh, C., Keskula, P., Mendoza-Villanueva, D., De La Vega, F.M., Kunz, P.L., Liao, J.C., Leppert, J.T., Sunwoo, J.B., Sabatti, C., Boehm, J.S., Hahn, W.C., Zheng, G.X.Y., Davis, M.M., Kuo, C.J. (2018). Organoid Modeling of the Tumor Immune Microenvironment. Cell *175*, 1972–1988.e16. doi: 10.1016/j.cell.2018.11.021; pmid: 30550791

45. Li, X., Nadauld, L., Ootani, A., Corney, D.C., Pai, R.K., Gevaert, O., Cantrell, M.A., Rack, P.G., Neal, J.T., Chan, C.W., Yeung, T., Gong, X., Yuan, J., Wilhelmy, J., Robine, S., Attardi, L.D., Plevritis, S.K., Hung, K.E., Chen, C.Z., Ji, H.P., Kuo, C.J. (2014). Oncogenic transformation of diverse gastrointestinal tissues in primary organoid culture. Nat. Med. *20*, 769–77. doi: 10.1038/nm.3585; pmid: 24859528

bioRxiv preprint doi: https://doi.org/10.1101/2022.11.29.516437; this version posted November 29, 2022. The copyright holder for this preprint (which was not certified by peer review) is the author/funder, who has granted bioRxiv a license to display the preprint in perpetuity. It is made available under aCC-BY-NC-ND 4.0 International license.

46. Kunst, A., Drager, B., and Ziegenhorn, J. (1983). UV methods with hexokinase and glucose-6- phosphate dehydrogenase. In Methods of Enzymatic Analysis (Academic Press), vol. 4, pp. 163–172.

47. Folch, J., Lees, M., and Sloane Stanley, G.H. (1957). A simple method for the isolation and purification of total lipids from animal tissues. J. Biol. Chem. *226*, 497–509. doi: 10.1016/S0021-9258(18)64849-5; pmid: 13428781

48. Fisher-Wellman, K.H., Davidson, M.T., Narowski. T.M., Lin, C.T., Koves T.R., and Muoio, D.M. (2018). Mitochondrial Diagnostics: A Multiplexed Assay Platform for Comprehensive Assessment of Mitochondrial Energy Fluxes. Cell Rep. *24*, 3593–3606. doi: 10.1016/j.celrep.2018.08.091; pmid: 30257218

49. Argus, J.P., Wilks, M.Q., Zhou, Q.D., Hsieh, W.Y., Khialeeva, E., Hoi, X.P., Bui, V., Xu, S., Yu, A.K., Wang, E.S., Herschman, H.R., Williams, K.J., and Bensinger, S.J. (2018). Development and Application of FASA, a Model for Quantifying Fatty Acid Metabolism Using Stable Isotope Labeling. Cell reports *25*, 2919–2934. doi: 10.1016/j.celrep.2018.11.041; pmid: 30517876

50. Murata, H., Hruz, P.W., and Mueckler, M. (2002). Indinavir inhibits the glucose transporter isoform Glut4 at physiologic concentrations. AIDS *16*, 859–863. doi: 10.1097/00002030-200204120-00005; pmid: 11919487

51. O'Brien, K.A., Horscroft, J.A., Devaux, J., Lindsay, R.T., Steel, A.S., Clark, A.D., Philp, A., Harridge, S.D.R., and Murray, A.J. (2019). PPARα-independent effects of nitrate supplementation on skeletal muscle metabolism in hypoxia. Biochim. Biophys. Acta. Mol. Basis Dis. *1865*, 844–853. doi: 10.1016/j.bbadis.2018.07.027; pmid: 30055294

52. Horscroft, J.A., O'Brien, K.A., Clark, A.D., Lindsay, R.T., Steel, A.S., Procter, N.E.K., Devaux, J., Frenneaux, M., Harridge, S.D.R., and Murray, A.J. (2019). Inorganic nitrate, hypoxia, and the regulation of cardiac mitochondrial respiration-probing the role of PPARα. FASEB J. *33*, 7563–7577. doi: 10.1096/fj.201900067R; pmid: 30870003

53. Kim, D., Langmead, B., and Salzberg, S.L. (2015). HISAT: a fast spliced aligner with low memory requirements. Nat. Methods *12*, 357–360. doi: 10.1038/nmeth.3317; pmid: 25751142

54. Anders, S., Pyl, P.T., and Huber, W. (2015). HTSeq-A Python framework to work with high-throughput sequencing data. Bioinformatics *31*, 166–169. doi: 10.1093/bioinformatics/btu638; pmid: 25260700

55. Love, M.I., Huber, W., and Anders, S. (2014). Moderated estimation of fold change and dispersion for RNA-seq data with DESeq2. Genome Biol. *15*, 550. doi: 10.1186/s13059-014-0550-8; pmid: 25516281

56. Sergushichev, A.A. (2016). An algorithm for fast preranked gene set enrichment analysis using cumulative statistic calculation. bioRxiv *060012*. doi: 10.1101/060012

57. Kanehisa, A. (2019). Toward understanding the origin and evolution of cellular organisms. Protein Sci. *28*, 1947–1951. doi: 10.1002/pro.3715; pmid: 31441146

58. Kanehisa, M., Furumichi, M., Sato, Y., Ishiguro-Watanabe, M., and Tanabe, M. (2021). KEGG: Integrating viruses and cellular organisms. Nucleic Acids Res. *49*, D545–D551. doi: 10.1093/nar/gkaa970; pmid: 33125081

59. Alvarez, M.J., Shen, Y., Giorgi, F.M., Lachmann, A., Ding, B.B., Ye, B.H., and Califano, A. (2016). Network-based inference of protein activity helps functionalize the genetic landscape of cancer. Nat. Genet. *48*, 838–847. doi: 10.1038/ng.3593; pmid: 27322546

60. Garcia-Alonso, L., Holland, C.H., Ibrahim, M.M., Turei, D., and Saez-Rodriguez, J. (2019). Benchmark and integration of resources for the estimation of human transcription factor activities. Genome Res. *29*, 1363–1375. doi: 10.1101/gr.240663.118; pmid: 31340985

61. Tucker, D.F., Sullivan, J.T., Mattia, K.A., Fisher, C.R., Barnes, T., Mabila, M.N., Wilf, R., Sulli, C., Pitts, M., Payne, R.J., Hall, M., Huston-Paterson, D., Deng, X., Davidson, E., Willis, S.H., Doranz, B.J., Chambers, R., and Rucker, J.B. (2018). Isolation of state-dependent monoclonal antibodies against the 12-transmembrane domain glucose transporter 4 using virus-like particles. Proc. Natl. Acad. Sci. USA *115*, E4990–E4999. doi: 10.1073/pnas.1716788115; pmid: 29769329

62. Hannan, N.R., Segeritz, C.P., Touboul, T., and Vallier, L. (2013). Production of hepatocyte-like cells from human pluripotent stem cells. Nat. Protoc. *8*, 430–437. doi: 10.1038/nprot.2012.153; pmid: 23424751

63. Mills R.J., Humphrey, S.J., Fortuna, P.R.J., Lor, M., Foster, S.R., Quaife-Ryan, G.A., Johnston, R.L., Dumenil, T., Bishop, C., Rudraraju, R., Rawle, D.J., Le, T., Zhao, W., Lee, L., Mackenzie-Kludas, C., Mehdiabadi, N.R., Halliday, C., Gilham, D., Fu, L., Nicholls, S.J., Johansson, J., Sweeney, M., Wong, N.C.W., Kulikowski, E., Sokolowski, K.A., Tse, B.W.C., Devilée, L., Voges, H.K., Reynolds, L.T., Krumeich, S., Mathieson, E., Abu-Bonsrah, D., Karavendzas, K., Griffen, B., Titmarsh, D., Elliott, D.A., McMahon, J., Suhrbier, A., Subbarao, K., Porrello, E.R., Smyth, M.J., Engwerda, C.R., MacDonald, K.P.A., Bald, T., James, D.E., and Hudson, J.E. (2021). BET inhibition blocks inflammation-induced cardiac dysfunction and SARS-CoV-2 infection. Cell *184*, 2167–2182. doi: 10.1016/j.cell.2021.03.026; pmid: 33811809

64. Mills, R.J., Titmarsh, D.M., Koenig, X., Parker, B.L., Ryall, J.G., Quaife-Ryan, G.A., Voges, H.K., Hodson, M.P., Ferguson, C., Drowley, L., Plowright, A.T., Needham, E.J., Wang, Q.D., Gregorevic, P., Xin, M., Thomas, W.G., Parton, R.G., Nielsen, L.K., Launikonis, B.S., James, D.E., Elliott, D.A., Porrello, E.R., and Hudson, J.E. (2017). Functional screening in human cardiac organoids reveals a metabolic mechanism for cardiomyocyte cell cycle arrest. Proc. Natl. Acad. Sci. USA *114*, E8372–E8381. doi: 10.1073/pnas.1707316114; pmid: 28916735

65. Mills, R.J., Parker, B.L., Quaife-Ryan, G.A., Voges, H.K., Needham, E.J., Bornot, A., Ding, M., Andersson, H., Polla, M., Elliott, D.A., Drowley, L., Clausen, M., Plowright, A.T., Barrett, I.P., Wang, Q.D., James, D.E., Porrello, E.R., and Hudson, J.E. (2019). Drug Screening in Human PSC-Cardiac Organoids Identifies Pro-proliferative Compounds Acting via the Mevalonate Pathway. Cell Stem Cell *24*, 895–907. doi: 10.1016/j.stem.2019.03.009; pmid: 30930147

66. Voges, H.K., Mills, R.J., Elliott, D.A., Parton, R.G., Porrello, E.R., and Hudson, J.E. (2017). Development of a human cardiac organoid injury model reveals innate regenerative potential. Development *144*, 1118–1127. doi: 10.1242/dev.143966; pmid: 28174241

67. Hudson, J.E., Titmarsh, D., Hidalgo, A., Wolvetang, E., and Cooper-White, J. (2012). Primitive cardiac cells from human embryonic stem cells. Stem Cells Dev. *21*, 1513–1523. doi: 10.1089/scd.2011.0254; pmid: 21933026